

Fundamental Limits of Wideband Localization— Part I: A General Framework

Yuan Shen, *Student Member, IEEE*, and Moe Z. Win, *Fellow, IEEE*

Abstract— The availability of positional information is of great importance in many commercial, public safety, and military applications. The coming years will see the emergence of location-aware networks with sub-meter accuracy, relying on accurate range measurements provided by wide bandwidth transmissions. In this two-part paper, we determine the fundamental limits of localization accuracy of wideband wireless networks in harsh multipath environments. We first develop a general framework to characterize the localization accuracy of a given node here and then extend our analysis to cooperative location-aware networks in Part II.

In this paper, we characterize localization accuracy in terms of a performance measure called the squared position error bound (SPEB), and introduce the notion of equivalent Fisher information to derive the SPEB in a succinct expression. This methodology provides insights into the essence of the localization problem by unifying localization information from individual anchors and information from a priori knowledge of the agent's position in a canonical form. Our analysis begins with the received waveforms themselves rather than utilizing only the signal metrics extracted from these waveforms, such as time-of-arrival and received signal strength. Hence, our framework exploits all the information inherent in the received waveforms, and the resulting SPEB serves as a fundamental limit of localization accuracy.

Index Terms—Cramér-Rao bound (CRB), equivalent Fisher information (EFI), information inequality, localization, ranging information (RI), squared position error bound (SPEB).

I. INTRODUCTION

Location-awareness plays a crucial role in many wireless network applications, such as localization services in next generation cellular networks [1], search-and-rescue operations [2], [3], logistics [4], and blue force tracking in battlefields [5]. The Global Positioning System (GPS) is the most important technology to provide location-awareness around the globe through a constellation of at least 24 satellites [6], [7]. However, the effectiveness of GPS is limited in harsh environments, such as in buildings, in urban canyons, under tree canopies, and in caves [8], [9], due to the inability of GPS signals to penetrate most obstacles. Hence, new localization techniques

Manuscript received April 17, 2008; revised October 10, 2008. Current version published Month Day 2010. This research was supported, in part, by the National Science Foundation under Grant ECCS-0901034, the Office of Naval Research Presidential Early Career Award for Scientists and Engineers (PECASE) N00014-09-1-0435, and MIT Institute for Soldier Nanotechnologies. The paper was presented in part at the IEEE Wireless Communications and Networking Conference, Hong Kong, March, 2007.

The authors are with the Laboratory for Information and Decision Systems (LIDS), Massachusetts Institute of Technology, 77 Massachusetts Avenue, Cambridge, MA 02139 USA (e-mail: {shenyuan, moewin}@mit.edu).

Communicated by Holger Boche, Associated Editor for Communications. Color versions of the figures in this paper are available online at <http://ieeexplore.ieee.org>.

Digital Object Identifier XXX.XXX

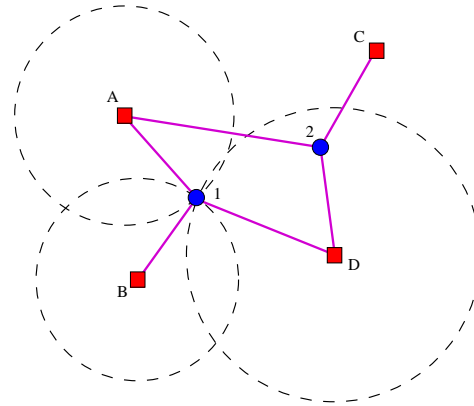


Fig. 1. Location-aware networks: the anchors (A, B, C, and D) communicate with the agents (1 and 2), and each edge denotes a connection link between anchor and agent.

are required to meet the increasing need for accurate localization in such harsh environments [8], [9].

Wideband wireless networks are capable of providing accurate localization in GPS-denied environments [8]–[12]. Wide bandwidth or ultra-wide bandwidth (UWB) signals are particularly well-suited for localization, since they can provide accurate and reliable range (distance) measurements due to their fine delay resolution and robustness in harsh environments [13]–[20]. For more information about UWB, we refer the reader to [21]–[26].

Location-aware networks generally consist of two kinds of nodes: anchors and agents. Anchors have known positions (for example, through GPS or system design), while agents have unknown positions and attempt to determine their positions (see Fig. 1). Each node is equipped with a wideband transceiver, and localization is accomplished through the use of radio communications between agents and their neighboring anchors. Localizing an agent requires a number of signals transmitted from the anchors, and the relative position of the agent can be inferred from these received waveforms using a variety of signal metrics. Commonly used signal metrics include time-of-arrival (TOA) [8], [9], [17]–[20], [27]–[30], time-difference-of-arrival (TDOA) [31], [32], angle-of-arrival (AOA) [9], [33], and received signal strength (RSS) [9], [34], [35].

Time-based metrics, TOA and TDOA, are obtained by measuring the signal propagation time between nodes. In ideal scenarios, the estimated distance equals the product of the known propagation speed and the measured signal propagation time. The TOA metric gives possible positions of an agent on a circle with the anchor at the center, and it can be obtained by

either the one-way time-of-flight of a signal in a synchronized network [18], [19], [28], [29], or the round-trip time-of-flight in a non-synchronized network [26], [36]. Alternatively, the TDOA metric provides possible positions of an agent on the hyperbola determined by the difference in the TOAs from two anchors located at the foci. Note that TDOA techniques require synchronization among anchors but not necessarily with the agent.

Another signal metric is AOA, the angle at which a signal arrives at the agent. The AOA metric can be obtained using an array of antennas, based on the signals' TOA at each antenna.¹ The use of AOA for localization has been investigated, and many hybrid systems have been proposed, including hybrid TOA/AOA systems [30], [41], and hybrid TDOA/AOA systems [42]. However, some of these studies employ narrowband signal models, which are not applicable for wideband antenna arrays. Others are restricted to far-field scenarios or use far-field assumptions.

RSS is also a useful metric that uses the strength of the received signal to estimate the propagation distance between nodes [9], [34], [36]. This metric can be measured during the data communications using low-complexity circuits. Although widely implemented, RSS has limited accuracy due to the difficulty in precisely modeling the relationship between the RSS and the propagation distance [4], [9].

Note that the signal metrics extracted from the received waveforms may discard relevant information for localization. Moreover, models for the signal metrics depend heavily on the specific measurement processes.² Therefore, in deriving the fundamental limits of localization accuracy, it is necessary to utilize the received waveforms rather than the signal metrics extracted from the waveforms [28], [29], [46], [47].

Since the received waveforms are affected by random phenomena such as noise, fading, shadowing, multipath, and non-line-of-sight (NLOS) propagations [48], [49], the agents' position estimates are subject to uncertainty. The Cramér-Rao bound (CRB) sets a lower bound on the variance of estimates for deterministic parameters [50], [51], and it has been used as a performance measure for localization accuracy [52]. However, relatively few studies have investigated the effect of multipath and NLOS propagations on localization accuracy. Multipath refers to a propagation phenomenon in which a transmitted signal reaches the receive antenna via multiple paths. The superposition of these arriving paths results in fading and interference. NLOS propagations, created by physical obstructions in the direct path, produce a positive bias in the propagation time and decrease the strength of the received signal, which can severely degrade the localization accuracy. Several types of methods have been proposed to deal with NLOS propagations: 1) treat NLOS biases as additive

noise injected in the true propagation distances [8], [53], [54];³ 2) identify and weigh the importance of NLOS signals for localization [55]–[60]; or 3) consider NLOS biases as parameters to be estimated [27]–[30], [46], [47], [61], [62]. The authors in [8], [9], [28], [29] showed that NLOS signals do not improve localization accuracy unless a priori knowledge of the NLOS biases is available, but their results were restricted to specific models or approximations. Moreover, detailed effects of multipath propagations on localization accuracy remains under-explored.

In this paper, we develop a general framework to determine the localization accuracy of wireless networks.⁴ Our analysis begins with the received waveforms themselves rather than utilizing only signal metrics extracted from the waveforms, such as TOA, TDOA, AOA, and RSS. The main contributions of this paper are as follows:

- We derive the fundamental limits of localization accuracy for wideband wireless networks, in terms of a performance measure called the *squared position error bound* (SPEB), in the presence of multipath and NLOS propagation.
- We propose the notion of *equivalent Fisher information* (EFI) to derive the agent's localization information. This approach unifies such information from different anchors in a canonical form as a weighed sum of the direction matrix associated with individual anchors with the weights characterizing the information intensity.
- We quantify the contribution of the *a priori knowledge* of the channel parameters and agent's position to the agent's localization information, and show that NLOS components can be beneficial when a priori channel knowledge is available.
- We derive the performance limits for localization systems employing *wideband antenna arrays*. The AOA metric obtained from antenna arrays are shown not to further improve the localization accuracy beyond that provided by TOA metric alone.
- We quantify the effect of *clock asynchronism* between anchors and agents on localization accuracy for networks where nodes employ a single antenna or an array of antennas.

The rest of the paper is organized as follows. Section II presents the system model, the notion of the SPEB, and the Fisher information matrix (FIM) for the SPEB. In Section III, we introduce the notion of EFI and show how it can help the derivation of the SPEB. In Section IV, we investigate the performance of localization systems employing wideband antenna arrays. Section V investigates the effect of clock asynchronism between anchors and agents. Discussions are provided in Section VI. Finally, numerical illustrations are given in Section VII, and conclusions are drawn in the last section.

¹The AOA metric can be obtained in two ways, directly through measurement by a directional antenna, or indirectly through TOA measurements using an antenna array [37]–[40]. Wideband directional antennas that satisfy size and cost requirements are difficult to implement, since they are required to perform across a large bandwidth [36]. As such, antenna arrays are more commonly used when angle measurement for wide bandwidth signals is necessary.

²For instance, the error of the TOA metric is commonly modeled as an additive Gaussian random variable [8], [30], [43]. This model contradicts the studies in [18]–[20], [44], [45], and the experimental results in [8], [16].

³In practice, however, a NLOS induced range bias can be as much as a few kilometers depending on the propagation environment [48], [55], and small perturbation may not compensate for NLOS induced error.

⁴In Part II [63], we extend our analysis to cooperative location-aware networks.

Notations: The notation $\mathbb{E}_{\mathbf{z}}\{\cdot\}$ is the expectation operator with respect to the random vector \mathbf{z} ; $\mathbf{A} \succeq \mathbf{B}$ denotes that the matrix $\mathbf{A} - \mathbf{B}$ is positive semi-definite; $\text{tr}\{\cdot\}$ is the trace of a square matrix; $[\cdot]_{n \times n}$ denotes the upper left $n \times n$ submatrix of its argument; $[\cdot]_{n,m}$ is the element at the n th row and m th column of its argument; $\|\cdot\|$ is the Euclidean norm of its argument; and the superscripts $[\cdot]^T$ represents the transpose of its argument. We denote by $f(\mathbf{x})$ the probability density function (PDF) $f_{\mathbf{X}}(\mathbf{x})$ of the random vector \mathbf{X} unless specified otherwise, and we also use in the paper the following function for the FIM:

$$\mathbf{F}_{\mathbf{z}}(\mathbf{w}; \mathbf{x}, \mathbf{y}) \triangleq \mathbb{E}_{\mathbf{z}} \left\{ \left[\frac{\partial}{\partial \mathbf{x}} \ln f(\mathbf{w}) \right] \left[\frac{\partial}{\partial \mathbf{y}} \ln f(\mathbf{w}) \right]^T \right\},$$

where \mathbf{w} can be either a vector or a symbol.⁵

II. SYSTEM MODEL

In this section, we describe the wideband channel model [14], [21], [24], [26], [64], formulate the problem, and briefly review the information inequality and Fisher information. We also introduce the squared position error bound, which is a fundamental limit of localization accuracy.

A. Signal Model

Consider a wireless network consisting of N_b anchors and multiple agents. Anchors have perfect knowledge of their positions, and each agent attempts to estimate its position based on the received waveforms from neighboring anchors (see Fig. 1).⁶ Wideband signals traveling from anchors to agents are subject to multipath propagation.

Let $\mathbf{p} \in \mathbb{R}^2$ denote the position of the agent,⁷ which is to be estimated. The set of anchors is denoted by $\mathcal{N}_b = \{1, 2, \dots, N_b\} \triangleq \mathcal{N}_L \cup \mathcal{N}_{NL}$, where \mathcal{N}_L denotes the set of anchors that provide LOS signals to the agent and \mathcal{N}_{NL} denotes the set of remaining anchors that provide NLOS signals to the agent. The position of anchor k is known and denoted by $\mathbf{p}_k \in \mathbb{R}^2$ ($k \in \mathcal{N}_b$). Let ϕ_k denote the angle from anchor k to the agent, i.e.,

$$\phi_k = \tan^{-1} \frac{y - y_k}{x - x_k},$$

where $\mathbf{p} \triangleq [x \ y]^T$ and $\mathbf{p}_k \triangleq [x_k \ y_k]^T$.

The received waveform at the agent from anchor k can be written as

$$r_k(t) = \sum_{l=1}^{L_k} \alpha_k^{(l)} s(t - \tau_k^{(l)}) + z_k(t), \quad t \in [0, T_{\text{ob}}], \quad (1)$$

where $s(t)$ is a known wideband waveform whose Fourier transform is denoted by $S(f)$, $\alpha_k^{(l)}$ and $\tau_k^{(l)}$ are the amplitude and delay, respectively, of the l th path, L_k is the number

of multipath components (MPCs), $z_k(t)$ represents the observation noise modeled as additive white Gaussian processes with two-side power spectral density $N_0/2$, and $[0, T_{\text{ob}}]$ is the observation interval. The relationship between the agent's position and the delays of the propagation paths is

$$\tau_k^{(l)} = \frac{1}{c} \left[\|\mathbf{p} - \mathbf{p}_k\| + b_k^{(l)} \right], \quad (2)$$

where c is the propagation speed of the signal, and $b_k^{(l)} \geq 0$ is a range bias. The range bias $b_k^{(1)} = 0$ for LOS propagation, whereas $b_k^{(l)} > 0$ for NLOS propagation.⁸

B. Error Bounds on Position Estimation

Our analysis is based on the received waveforms given by (1), and hence the parameter vector $\boldsymbol{\theta}$ includes the agent's position and the nuisance multipath parameters [9], [62], i.e.,

$$\boldsymbol{\theta} = \left[\mathbf{p}^T \quad \boldsymbol{\kappa}_1^T \quad \boldsymbol{\kappa}_2^T \quad \cdots \quad \boldsymbol{\kappa}_{N_b}^T \right]^T,$$

where $\boldsymbol{\kappa}_k$ is the vector of the multipath parameters associated with $r_k(t)$, given by

$$\boldsymbol{\kappa}_k = \begin{cases} \left[\alpha_k^{(1)} & b_k^{(2)} & \alpha_k^{(2)} & \cdots & b_k^{(L_k)} & \alpha_k^{(L_k)} \right]^T, & k \in \mathcal{N}_L, \\ \left[b_k^{(1)} & \alpha_k^{(1)} & b_k^{(2)} & \alpha_k^{(2)} & \cdots & b_k^{(L_k)} & \alpha_k^{(L_k)} \right]^T, & k \in \mathcal{N}_{NL}. \end{cases}$$

Note that $b_k^{(1)} = 0$ for $k \in \mathcal{N}_L$ and is excluded from $\boldsymbol{\kappa}_k$.

We introduce \mathbf{r} as the vector representation of all the received waveforms $r_k(t)$, given by

$$\mathbf{r} = \left[\mathbf{r}_1^T \quad \mathbf{r}_2^T \quad \cdots \quad \mathbf{r}_{N_b}^T \right]^T,$$

where \mathbf{r}_k is obtained from the Karhunen-Loeve expansion of $r_k(t)$ [50], [51]. Let $\hat{\boldsymbol{\theta}}$ denote an estimate of the parameter vector $\boldsymbol{\theta}$ based on observation \mathbf{r} . The mean squared error (MSE) matrix of $\hat{\boldsymbol{\theta}}$ satisfies the information inequality [50], [51], [65]

$$\mathbb{E}_{\mathbf{r}, \boldsymbol{\theta}} \left\{ (\hat{\boldsymbol{\theta}} - \boldsymbol{\theta})(\hat{\boldsymbol{\theta}} - \boldsymbol{\theta})^T \right\} \succeq \mathbf{J}_{\boldsymbol{\theta}}^{-1}. \quad (3)$$

where $\mathbf{J}_{\boldsymbol{\theta}}$ is the Fisher information matrix (FIM) for the parameter vector $\boldsymbol{\theta}$.⁹ Let $\hat{\mathbf{p}}$ be an estimate of the agent's position, and it follows from (3) that¹⁰

$$\mathbb{E}_{\mathbf{r}, \boldsymbol{\theta}} \left\{ (\hat{\mathbf{p}} - \mathbf{p})(\hat{\mathbf{p}} - \mathbf{p})^T \right\} \succeq [\mathbf{J}_{\boldsymbol{\theta}}^{-1}]_{2 \times 2},$$

⁸LOS propagation does not introduce a range bias because there is an unblocked direct path. NLOS propagation introduces a positive range bias because such signals either reflect off objects or penetrate through obstacles. In this paper, received signals whose first path undergoes LOS propagation are referred to as LOS signals, otherwise these signals are referred to as NLOS signals.

⁹When a subset of parameters is random, $\mathbf{J}_{\boldsymbol{\theta}}$ is called the Bayesian information matrix. Inequality (3) also holds under some regularity conditions and provides lower bound on the MSE matrix of any unbiased estimates of the deterministic parameters and any estimates of the random parameters [50], [65]. With a slight abuse of notation, $\mathbb{E}_{\mathbf{r}, \boldsymbol{\theta}}\{\cdot\}$ will be used for deterministic, hybrid, Bayesian cases with the understanding that the expectation operation is not performed over the deterministic components of $\boldsymbol{\theta}$.

¹⁰Note that for three-dimensional localization, we need to consider a 3×3 matrix $[\mathbf{J}_{\boldsymbol{\theta}}^{-1}]_{3 \times 3}$.

⁵For example, \mathbf{w} is replaced by symbol $\mathbf{r}|\boldsymbol{\theta}$ in the case that $f(\cdot)$ is a conditional PDF of \mathbf{r} given $\boldsymbol{\theta}$.

⁶Agents estimate their positions independently, and hence without loss of generality, our analysis focuses on one agent.

⁷We first focus on two dimensional cases and then extend the results to three-dimensional cases where $\mathbf{p} \in \mathbb{R}^3$.

and hence

$$\mathbb{E}_{\mathbf{r},\boldsymbol{\theta}} \{ \|\hat{\mathbf{p}} - \mathbf{p}\|^2 \} \geq \text{tr} \left\{ [\mathbf{J}_{\boldsymbol{\theta}}^{-1}]_{2 \times 2} \right\}. \quad (4)$$

Therefore, we define the right hand side of (4) as a measure to characterize the limits of position accuracy as follows.

Definition 1 (Squared Position Error Bound): The squared position error bound (SPEB) is defined to be

$$\mathcal{P}(\mathbf{p}) \triangleq \text{tr} \left\{ [\mathbf{J}_{\boldsymbol{\theta}}^{-1}]_{2 \times 2} \right\}.$$

C. Fisher Information Matrix

In this section, we derive the FIM for both deterministic and random parameter estimation to evaluate the SPEB.

1) *FIM without A Priori Knowledge:* The FIM for the deterministic parameter vector $\boldsymbol{\theta}$ is given by [50]

$$\mathbf{J}_{\boldsymbol{\theta}} = \mathbf{F}_{\mathbf{r}}(\mathbf{r}|\boldsymbol{\theta}; \boldsymbol{\theta}, \boldsymbol{\theta}), \quad (5)$$

where $f(\mathbf{r}|\boldsymbol{\theta})$ is the likelihood ratio of the random vector \mathbf{r} conditioned on $\boldsymbol{\theta}$. Since the received waveforms from different anchors are independent, the likelihood ratio can be written as [51]

$$f(\mathbf{r}|\boldsymbol{\theta}) = \prod_{k \in \mathcal{N}_b} f(\mathbf{r}_k|\boldsymbol{\theta}), \quad (6)$$

where

$$f(\mathbf{r}_k|\boldsymbol{\theta}) \propto \exp \left\{ \frac{2}{N_0} \int_0^{T_{\text{ob}}} r_k(t) \sum_{l=1}^{L_k} \alpha_k^{(l)} s(t - \tau_k^{(l)}) dt - \frac{1}{N_0} \int_0^{T_{\text{ob}}} \left[\sum_{l=1}^{L_k} \alpha_k^{(l)} s(t - \tau_k^{(l)}) \right]^2 dt \right\}.$$

Substituting (6) in (5), we have the FIM $\mathbf{J}_{\boldsymbol{\theta}}$ as

$$\mathbf{J}_{\boldsymbol{\theta}} = \frac{1}{c^2} \begin{bmatrix} \mathbf{T}_L \boldsymbol{\Lambda}_L \mathbf{T}_L^T + \mathbf{T}_{NL} \boldsymbol{\Lambda}_{NL} \mathbf{T}_{NL}^T & \mathbf{T}_{NL} \boldsymbol{\Lambda}_{NL} \\ \boldsymbol{\Lambda}_{NL} \mathbf{T}_{NL}^T & \boldsymbol{\Lambda}_{NL} \end{bmatrix}, \quad (7)$$

where $\boldsymbol{\Lambda}_L$, \mathbf{T}_L , $\boldsymbol{\Lambda}_{NL}$, and \mathbf{T}_{NL} are given by (41) and (42). In the above matrices, $\boldsymbol{\Lambda}_L$ and \mathbf{T}_L are related to the LOS signals, and $\boldsymbol{\Lambda}_{NL}$ and \mathbf{T}_{NL} are related to the NLOS signals.

2) *FIM with A Priori Knowledge:* We now incorporate the a priori knowledge of the agent's position and channel parameters for localization. Since the multipath parameters $\boldsymbol{\kappa}_k$ are independent a priori, the PDF of $\boldsymbol{\theta}$ can be expressed as¹¹

$$f(\boldsymbol{\theta}) = f(\mathbf{p}) \prod_{k \in \mathcal{N}_b} f(\boldsymbol{\kappa}_k|\mathbf{p}), \quad (8)$$

where $f(\mathbf{p})$ is the PDF of the agent's position, and $f(\boldsymbol{\kappa}_k|\mathbf{p})$ is the joint PDF of the multipath parameter vector $\boldsymbol{\kappa}_k$ conditioned on the agent's position. Based on the models of wideband channels [36], [40], [64] and UWB channels [14], [21], [24], [26], [36], we derive $f(\boldsymbol{\kappa}_k|\mathbf{p})$ in (53) in Appendix B and show that

$$f(\boldsymbol{\kappa}_k|\mathbf{p}) = f(\boldsymbol{\kappa}_k|d_k), \quad (9)$$

where $d_k = \|\mathbf{p} - \mathbf{p}_k\|$.

¹¹When a subset of parameters are deterministic, they are eliminated from $f(\boldsymbol{\theta})$.

The joint PDF of observation and parameters can be written as

$$f(\mathbf{r}, \boldsymbol{\theta}) = f(\mathbf{r}|\boldsymbol{\theta}) f(\boldsymbol{\theta}),$$

where $f(\mathbf{r}|\boldsymbol{\theta})$ is given by (6), and hence the FIM becomes

$$\mathbf{J}_{\boldsymbol{\theta}} = \mathbf{J}_w + \mathbf{J}_p, \quad (10)$$

where $\mathbf{J}_w \triangleq \mathbf{F}_{\mathbf{r},\boldsymbol{\theta}}(\mathbf{r}|\boldsymbol{\theta}; \boldsymbol{\theta}, \boldsymbol{\theta})$ and $\mathbf{J}_p \triangleq \mathbf{F}_{\boldsymbol{\theta}}(\boldsymbol{\theta}; \boldsymbol{\theta}, \boldsymbol{\theta})$ are the FIMs from the observations and the a priori knowledge, respectively.¹² The FIM \mathbf{J}_w can be obtained by taking the expectation of $\mathbf{J}_{\boldsymbol{\theta}}$ in (7) over the random parameter vector $\boldsymbol{\theta}$, and \mathbf{J}_p can be obtained by substituting (8) in (10) as

$$\mathbf{J}_p = \begin{bmatrix} \boldsymbol{\Xi}_p + \sum_{k \in \mathcal{N}_b} \boldsymbol{\Xi}_{p,p}^k & \boldsymbol{\Xi}_{p,\boldsymbol{\kappa}}^1 & \cdots & \boldsymbol{\Xi}_{p,\boldsymbol{\kappa}}^{N_b} \\ [\boldsymbol{\Xi}_{p,\boldsymbol{\kappa}}^1]^T & \boldsymbol{\Xi}_{\boldsymbol{\kappa},\boldsymbol{\kappa}}^1 & & \mathbf{0} \\ \vdots & & \ddots & \\ [\boldsymbol{\Xi}_{p,\boldsymbol{\kappa}}^{N_b}]^T & \mathbf{0} & & \boldsymbol{\Xi}_{\boldsymbol{\kappa},\boldsymbol{\kappa}}^{N_b} \end{bmatrix}, \quad (11)$$

where $\boldsymbol{\Xi}_p$ describes the FIM from the a priori knowledge of \mathbf{p} , given by

$$\boldsymbol{\Xi}_p = \mathbf{F}_{\boldsymbol{\theta}}(\mathbf{p}; \mathbf{p}, \mathbf{p}),$$

and $\boldsymbol{\Xi}_{\boldsymbol{\kappa},\boldsymbol{\kappa}}^k = \mathbf{F}_{\boldsymbol{\theta}}(\boldsymbol{\kappa}_k|\mathbf{p}; \boldsymbol{\kappa}_k, \boldsymbol{\kappa}_k)$, $\boldsymbol{\Xi}_{p,p}^k = \mathbf{F}_{\boldsymbol{\theta}}(\boldsymbol{\kappa}_k|\mathbf{p}; \mathbf{p}, \mathbf{p})$, and $\boldsymbol{\Xi}_{p,\boldsymbol{\kappa}}^k = \mathbf{F}_{\boldsymbol{\theta}}(\boldsymbol{\kappa}_k|\mathbf{p}; \mathbf{p}, \boldsymbol{\kappa}_k)$ characterize the joint a priori knowledge of \mathbf{p} and $\boldsymbol{\kappa}_k$.

D. Equivalent Fisher Information Matrix

Determining the SPEB requires inverting the FIM $\mathbf{J}_{\boldsymbol{\theta}}$ in (7) and (10). However, $\mathbf{J}_{\boldsymbol{\theta}}$ is a matrix of high dimensions, while only a small submatrix $[\mathbf{J}_{\boldsymbol{\theta}}^{-1}]_{2 \times 2}$ is of interest. To circumvent direction matrix inversion and gain insights into the localization problem, we first introduce the notions of EFI [46], [47].

Definition 2 (Equivalent Fisher Information Matrix):

Given a parameter $\boldsymbol{\theta} = [\boldsymbol{\theta}_1^T \boldsymbol{\theta}_2^T]^T$ and the FIM $\mathbf{J}_{\boldsymbol{\theta}}$ of the form

$$\mathbf{J}_{\boldsymbol{\theta}} = \begin{bmatrix} \mathbf{A} & \mathbf{B} \\ \mathbf{B}^T & \mathbf{C} \end{bmatrix}, \quad (12)$$

where $\boldsymbol{\theta} \in \mathbb{R}^N$, $\boldsymbol{\theta}_1 \in \mathbb{R}^n$, $\mathbf{A} \in \mathbb{R}^{n \times n}$, $\mathbf{B} \in \mathbb{R}^{n \times (N-n)}$, and $\mathbf{C} \in \mathbb{R}^{(N-n) \times (N-n)}$ with $n < N$, the equivalent Fisher information matrix (EFIM) for $\boldsymbol{\theta}_1$ is given by¹³

$$\mathbf{J}_e(\boldsymbol{\theta}_1) \triangleq \mathbf{A} - \mathbf{B}\mathbf{C}^{-1}\mathbf{B}^T. \quad (13)$$

Note that the EFIM retains all the necessary information to derive the information inequality for the parameter vector $\boldsymbol{\theta}_1$, since $[\mathbf{J}_{\boldsymbol{\theta}}^{-1}]_{n \times n} = \mathbf{J}_e^{-1}(\boldsymbol{\theta}_1)$,¹⁴ and the MSE matrix of the estimates for $\boldsymbol{\theta}_1$ is bounded below by $\mathbf{J}_e^{-1}(\boldsymbol{\theta}_1)$.¹⁵ For two-dimensional localization ($n = 2$), we aim to reduce the dimension of the original FIM to the 2×2 EFIM.

¹²Note that $\mathbf{J}_{\boldsymbol{\theta}}$ in (10) requires averaging over the random parameters, and hence does not depend on any particular value of $\boldsymbol{\theta}$. In contrast, $\mathbf{J}_{\boldsymbol{\theta}}$ in (5) is a function of a particular value of the deterministic parameter vector $\boldsymbol{\theta}$.

¹³Note that $\mathbf{J}_e(\boldsymbol{\theta}_1)$ does not depend on any particular value of $\boldsymbol{\theta}_1$ for a random parameter vector $\boldsymbol{\theta}_1$, whereas it is a function of $\boldsymbol{\theta}_1$ for a deterministic parameter vector $\boldsymbol{\theta}_1$.

¹⁴The right hand side of (13) is known as the Schur complement of the matrix \mathbf{C} [66].

¹⁵When $\boldsymbol{\theta}_1 \in \mathbb{R}^1$, the EFIM has only one element since $J_e(\boldsymbol{\theta}_1)$ is a scalar.

III. EVALUATION OF EFIM

In this section, we apply the notion of equivalent Fisher information (EFI) to derive the SPEB for both the case with and without a priori knowledge. We also introduce the notion of ranging information (RI), which turns out to be the basic component of the SPEB.

A. EFIM without A Priori Knowledge

First consider a case in which a priori knowledge is unavailable. We apply the notion of EFI to reduce the dimension of the original FIM in (7), and the EFIM for the agent's position is presented in the following proposition.

Proposition 1: When a priori knowledge is unavailable, an EFIM for the agent's position is

$$\mathbf{J}_e(\mathbf{p}, \{\kappa_k : k \in \mathcal{N}_L\}) = \frac{1}{c^2} \mathbf{T}_L \mathbf{\Lambda}_L \mathbf{T}_L^T, \quad (14)$$

where \mathbf{T}_L and $\mathbf{\Lambda}_L$ are given by (41) and (42), respectively.

Proof: Let $\mathbf{A} = \mathbf{T}_{NL} \mathbf{\Lambda}_{NL} \mathbf{T}_{NL}^T + \mathbf{T}_L \mathbf{\Lambda}_L \mathbf{T}_L^T$, $\mathbf{B} = \mathbf{T}_{NL} \mathbf{\Lambda}_{NL}$, and $\mathbf{C} = \mathbf{\Lambda}_{NL}$ in (7). Applying the notion of EFI in (13) leads to the result. \square

Remark 1: When a priori knowledge is unavailable, NLOS signals do not contribute to the EFIM for the agent's position. Hence we can eliminate these NLOS signals when analyzing localization accuracy. This observation agrees with the results of [29], but the amplitudes of the MPCs are assumed to be known in their model.

Note that the dimension of the EFIM in (14) is much larger than 2×2 . We will apply the notion of EFI again to further reduce the dimension of the EFIM in the following theorem. Before the theorem, we introduce the notion of the first contiguous-cluster and ranging information (RI).

Definition 3 (First Contiguous-Cluster): The first contiguous-cluster is defined to be the set of paths $\{1, 2, \dots, j\}$, such that $|\tau_i - \tau_{i+1}| < T_s$ for $i = 1, 2, \dots, j-1$, and $|\tau_j - \tau_{j+1}| > T_s$, where T_s is the duration of $s(t)$.

Definition 4 (Ranging Information): The ranging information (RI) is a 2×2 matrix of the form $\lambda \mathbf{J}_r(\phi)$, where λ is a nonnegative number called the ranging information intensity (RII), and $\mathbf{J}_r(\phi)$ a 2×2 matrix called the ranging direction matrix (RDM) with angle ϕ , given by

$$\mathbf{J}_r(\phi) \triangleq \begin{bmatrix} \cos^2 \phi & \cos \phi \sin \phi \\ \cos \phi \sin \phi & \sin^2 \phi \end{bmatrix}.$$

The first contiguous-cluster is the first group of non-disjoint paths (see Fig. 2).¹⁶ The RDM is one-dimensional along the direction ϕ with unit intensity, i.e., $\mathbf{J}_r(\phi)$ has one (and only one) non-zero eigenvalue equal to 1 with corresponding eigenvector $\mathbf{q} = [\cos \phi \quad \sin \phi]^T$.

Theorem 1: When a priori knowledge is unavailable, the EFIM for the agent's position is a 2×2 matrix

$$\mathbf{J}_e(\mathbf{p}) = \sum_{k \in \mathcal{N}_L} \lambda_k \mathbf{J}_r(\phi_k), \quad (15)$$

¹⁶The first contiguous-cluster, defined for general wideband received signals, may contain many MPCs. Two paths that arrive at time τ_i and τ_j are called non-disjointed if $|\tau_i - \tau_j| < T_s$.

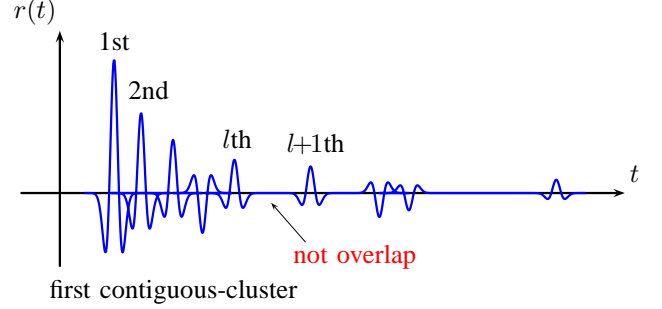


Fig. 2. An illustration of the first contiguous-cluster (containing l paths) in a LOS signal.

where λ_k is the RII from anchor k , given by

$$\lambda_k = \frac{8\pi^2 \beta^2}{c^2} (1 - \chi_k) \text{SNR}_k^{(1)}. \quad (16)$$

In (16), $0 \leq \chi_k \leq 1$ is given by (61),

$$\beta \triangleq \left(\frac{\int_{-\infty}^{+\infty} f^2 |S(f)|^2 df}{\int_{-\infty}^{+\infty} |S(f)|^2 df} \right)^{1/2}, \quad (17)$$

and

$$\text{SNR}_k^{(l)} \triangleq \frac{|\alpha_k^{(l)}|^2 \int_{-\infty}^{+\infty} |S(f)|^2 df}{N_0}. \quad (18)$$

Furthermore, only the first contiguous-cluster of LOS signals contains information for localization.

Proof: See Appendix C-A. \square

Remark 2: In Theorem 1, β is known as the *effective bandwidth* [50], [67], χ_k is called *path-overlap coefficient* (POC) that characterizes the effect of multipath propagation for localization, and $\text{SNR}_k^{(l)}$ is the SNR of the l th path in $r_k(t)$. We draw the following observations from Theorem 1:

- The original FIM in (7) can be transformed into a simple 2×2 EFIM in a canonical form, given by (15), as a weighted sum of the RDM from individual anchors. Each anchor (e.g. anchor k) can provide only one-dimensional RI along the direction ϕ_k , from the anchor to the agent, with intensity λ_k .¹⁷
- The RII λ_k depends on the effective bandwidth of $s(t)$, the SNR of the first path, and the POC. Since $0 \leq \chi_k \leq 1$, path-overlap in the first contiguous-cluster will reduce the RII, thus leading to a higher SPEB, unless the signal via the first path does not overlap with others ($\chi_k = 0$).
- The POC χ_k in (61) is determined only by the waveform $s(t)$ and the NLOS biases of the MPCs in the first contiguous-cluster. The independence of χ_k on the path amplitudes seems counter-intuitive. However, this is due to the fact that, although large $\alpha_k^{(l)}$ causes severe interpath interference for estimating the TOA $\tau_k^{(1)}$, it increases

¹⁷For notational convenience, we suppress the dependence of ϕ_k and λ_k on the agent's position \mathbf{p} throughout the paper.

the estimation accuracy for $\tau_k^{(l)}$, which in turn helps to mitigate the interpath interference.

We can specialize the above theorem into a case in which the first path in a LOS signal is completely resolvable, i.e., the first contiguous-cluster contains only a single component.

Corollary 1: When a priori knowledge is unavailable and the first contiguous-cluster of the received waveform from anchor k contains only the first path, the RII becomes

$$\lambda_k = \frac{8\pi^2\beta^2}{c^2} \text{SNR}_k^{(1)}. \quad (19)$$

Proof: See Appendix C-B. \square

Remark 3: When the first path is resolvable, $\chi_k = 0$ in (16) and hence λ_k attains its maximum value. However, when the signal via other paths overlap with the first one, these paths will degrade the estimation accuracy of the first path's arrival time and hence the RII. Corollary 1 is intuitive and important: the RII of a LOS signal depends only on the first path if the first path is resolvable. In such a case, all other paths can be eliminated, and the multipath signal is equivalent to a signal with only the first path for localization.

From Theorem 1, the SPEB can be derived in (20) shown at the bottom of the page. When the first paths are resolvable, by Corollary 1, we have all $\chi_k = 0$ in (20) and the corresponding $\mathcal{P}(\mathbf{p})$ becomes the same as those based on single-path signal models in [9], [29]. However, those results are not accurate when the first path is not resolvable.

B. EFIM with A Priori Knowledge

We now consider the case where there is a priori knowledge of the channel parameters, but not of the agent's position. In such cases, since \mathbf{p} is deterministic but unknown, $f(\mathbf{p})$ is eliminated in (8). Similar to the analysis in the previous section, we can derive the 2×2 EFIM for the corresponding FIM in (10).

Theorem 2: When a priori knowledge of the channel parameters is available and the sets of channel parameters corresponding to different anchors are mutually independent, the EFIM for the agent's position is a 2×2 matrix

$$\mathbf{J}_e(\mathbf{p}) = \sum_{k \in \mathcal{N}_L} \lambda_k \mathbf{J}_r(\phi_k) + \sum_{k \in \mathcal{N}_{NL}} \lambda_k \mathbf{J}_r(\phi_k), \quad (21)$$

where λ_k is given by (65a) for LOS signals and (65b) for NLOS signals.

Proof: See Appendix C-C. \square

Remark 4: Theorem 2 generalizes the result of Theorem 1 from deterministic to hybrid parameter estimation.¹⁸ In this case, the EFIM can still be expressed in a canonical form as a weighed sum of the RDMs from individual anchors. Note that due to the existence of a priori channel knowledge, the

¹⁸This is the case where the agent's position \mathbf{p} is deterministic and the channel parameters are random.

RII of NLOS signals can be positive, and hence these signals contribute to the EFIM as opposed to the case in Theorem 1.

Corollary 2: A priori channel knowledge increases the RII. In the absence of such knowledge, the expressions of RII in (65a) and (65b) reduce to (16) and zero, respectively.

Proof: See Appendix C-D. \square

Corollary 3: LOS signals can be treated as NLOS signals with infinite a priori Fisher information of $b_k^{(1)}$, i.e., $b_k^{(1)}$ is known. Mathematically, (65a) is equivalent to (65b) with $\mathbf{F}_\theta(\theta; b_k^{(1)}, b_k^{(1)}) \rightarrow \infty$.

Proof: See Appendix C-E. \square

Remark 5: Corollary 2 shows that Theorem 2 degenerates to Theorem 1 when a priori channel knowledge is unavailable. Moreover, Corollary 3 unifies the LOS and NLOS signals under the Bayesian estimation framework: the NLOS biases $b_k^{(1)}$ ($k \in \mathcal{N}_L$) can be regarded as random parameters with infinite a priori Fisher information instead of being eliminated from θ as in Section II-A. Hence, all of the signals can be modeled as NLOS, and infinite a priori Fisher information of $b_k^{(1)}$ will be assigned for LOS signals.

We next consider the case where a priori knowledge of the agent's position is available in addition to channel parameters. Note that the topology of the anchors and the agent changes with the position of the agent. The 2×2 EFIM is given in (67), which is more intricate than the previous two cases. To gain some insights, we consider a special case where¹⁹

$$\mathbb{E}_{\mathbf{p}} \{g(\mathbf{p})\} = g(\bar{\mathbf{p}}), \quad (22)$$

in which $\bar{\mathbf{p}} = \mathbb{E}_{\mathbf{p}} \{\mathbf{p}\}$ is the agent's expected position, for some function $g(\cdot)$ involved in the derivation of the EFIM (see Appendix C-F).

Proposition 2: When the a priori position distribution of the agent satisfies (22), and the sets of channel parameters corresponding to different anchors are mutually independent, the EFIM for the agent's position is a 2×2 matrix

$$\mathbf{J}_e(\mathbf{p}) = \sum_{k \in \mathcal{N}_b} \bar{\lambda}_k \mathbf{J}_r(\bar{\phi}_k) + \bar{\Xi}_{\mathbf{p}}, \quad (23)$$

where $\bar{\lambda}_k$ is given by (68), and $\bar{\phi}_k$ is the angle from anchor k to $\bar{\mathbf{p}}$.

Proof: See Appendix C-F. \square

Remark 6: The a priori knowledge of the agent's position is exploited, in addition to that of the channel parameters, for localization in Proposition 2. The expressions for the EFIM can be involved in general. Fortunately, if (22) is satisfied, the EFIM can be simply written as the sum of two parts as shown in (23): a weighted sum of the RDMs from individual anchors as in the previous two cases, and the EFIM from

¹⁹This occurs when the agent's a priori position distribution is concentrated in a small area relative to the distance between the agent and the anchors, so that $g(\mathbf{p})$ is flat in that area. For example, this condition is satisfied in far-field scenarios.

$$\mathcal{P}(\mathbf{p}) = \frac{c^2}{8\pi^2\beta^2} \frac{2 \sum_{k \in \mathcal{N}_L} (1 - \chi_k) \text{SNR}_k^{(1)}}{\sum_{k \in \mathcal{N}_L} \sum_{m \in \mathcal{N}_L} (1 - \chi_k)(1 - \chi_m) \text{SNR}_k^{(1)} \text{SNR}_m^{(1)} \sin^2(\phi_k - \phi_m)} \quad (20)$$

the a priori knowledge of the agent's position. This result unifies the contribution from anchors and that from the a priori knowledge of the agent's position into the EFIM. The concept of localization with a priori knowledge of the agent's position is useful for a wide range of applications such as successive localization or tracking.

IV. WIDEBAND LOCALIZATION WITH ANTENNA ARRAYS

In this section, we consider localization systems using wideband antenna arrays, which can perform both TOA and AOA measurements. Since the orientation of the array may be unknown, we propose a model to jointly estimate the agent's position and orientation, and derive the SPEB and the *squared orientation error bound* (SOEB).

A. System Model and Squared Orientation Error Bound

Consider a network where each agent is equipped with an N_a -antenna array,²⁰ which can extract both the TOA and AOA information with respect to neighboring anchors. Let $\mathcal{N}_a = \{1, 2, \dots, N_a\}$ denote the set of antennas, and let $\mathbf{p}_n^{\text{Array}} \triangleq [x_n^{\text{Array}} \ y_n^{\text{Array}}]^T$ denote the position of the agent's n th antenna, which needs to be estimated. Let ϕ_{nk} denote the angle from anchor k to the n th antenna, i.e.,

$$\phi_{nk} = \tan^{-1} \frac{y_n^{\text{Array}} - y_k}{x_n^{\text{Array}} - x_k}.$$

Since relative positions of the antennas in the array are usually known, if we denote $\mathbf{p} = [x \ y]^T$ as a reference point and φ as the orientation of the array,²¹ then the position of the n th antenna in the array can be represented as (Fig. 3)

$$\mathbf{p}_n^{\text{Array}} = \mathbf{p} + \begin{bmatrix} \Delta x_n(\mathbf{p}, \varphi) \\ \Delta y_n(\mathbf{p}, \varphi) \end{bmatrix}, \quad n \in \mathcal{N}_a,$$

where $\Delta x_n(\mathbf{p}, \varphi)$ and $\Delta y_n(\mathbf{p}, \varphi)$ denote the relative distance in x and y direction from the reference point to the n th antenna, respectively.

Since the array orientation may be unknown, we classify the localization problem into *orientation-aware* and *orientation-unaware* cases, where φ can be thought of as a random parameter with infinite (orientation-aware) and zero (orientation-unaware) a priori Fisher information [46].

The received waveform at the agent's n th antenna from anchor k can be written as

$$r_{nk}(t) = \sum_{l=1}^{L_{nk}} \alpha_{nk}^{(l)} s(t - \tau_{nk}^{(l)}) + z_{nk}(t), \quad t \in [0, T_{\text{ob}}],$$

where $\alpha_{nk}^{(l)}$ and $\tau_{nk}^{(l)}$ are the amplitude and delay, respectively, of the l th path, L_{nk} is the number of MPCs, and $z_{nk}(t)$ represents the observation noise modeled as additive white Gaussian processes with two-side power spectral density $N_0/2$. The

²⁰Each anchor has only one antenna here. We will discuss the case of multiple antennas on anchors at the end of this section.

²¹Note from geometry that the orientation φ is independent of the specific reference point.

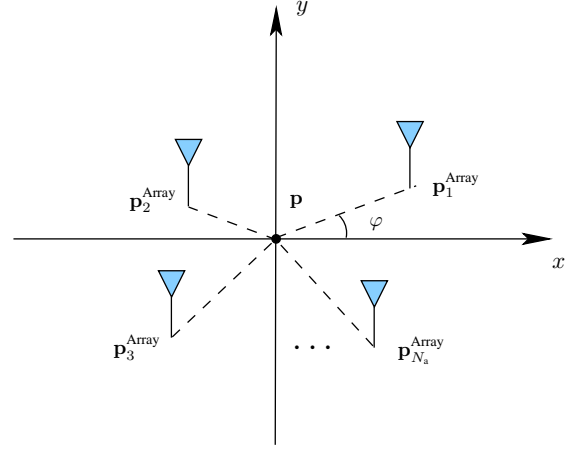


Fig. 3. An antenna array is described by the reference point \mathbf{p} , the orientation φ , and the relative positions of the antennas.

relationship between the position of the n th antenna and the delay of the l th path is

$$\tau_{nk}^{(l)} = \frac{1}{c} \left[\|\mathbf{p}_n^{\text{Array}} - \mathbf{p}_k\| + b_{nk}^{(l)} \right]. \quad (24)$$

The parameters to be considered include the position of the reference point, the array orientation, and the nuisance multipath parameter as

$$\boldsymbol{\theta} = \left[\mathbf{p}^T \quad \varphi \quad \check{\boldsymbol{\kappa}}_1^T \quad \check{\boldsymbol{\kappa}}_2^T \quad \dots \quad \check{\boldsymbol{\kappa}}_{N_a}^T \right]^T, \quad (25)$$

where $\check{\boldsymbol{\kappa}}_n$ consists of the multipath parameters associated with the received waveforms from all anchors at the n th antenna,

$$\check{\boldsymbol{\kappa}}_n = \left[\boldsymbol{\kappa}_{n,1}^T \quad \boldsymbol{\kappa}_{n,2}^T \quad \dots \quad \boldsymbol{\kappa}_{n,N_b}^T \right]^T,$$

and each $\boldsymbol{\kappa}_{nk}$ consists of the multipath parameters associated with $r_{nk}(t)$,

$$\boldsymbol{\kappa}_{nk} = \left[b_{nk}^{(1)} \quad \alpha_{nk}^{(1)} \quad \dots \quad b_{nk}^{(L_{nk})} \quad \alpha_{nk}^{(L_{nk})} \right]^T.$$

Similar to Section II-B, the overall received waveforms at the antenna array can be represented, using the KL expansion, by $\mathbf{r} = [\mathbf{r}_1^T \ \mathbf{r}_2^T \ \dots \ \mathbf{r}_{N_a}^T]^T$, where

$$\mathbf{r}_n = \left[\mathbf{r}_{n,1}^T \quad \mathbf{r}_{n,2}^T \quad \dots \quad \mathbf{r}_{n,N_b}^T \right]^T,$$

in which \mathbf{r}_{nk} is obtained by the KL expansion of $r_{nk}(t)$.

Definition 5 (Squared Orientation Error Bound): The squared orientation error bound (SOEB) is defined to be

$$\mathcal{P}(\varphi) \triangleq [\mathbf{J}_{\boldsymbol{\theta}}^{-1}]_{3,3}.$$

B. EFIM without A Priori Knowledge

We first consider scenarios in which a priori knowledge is unavailable. Following similar steps in Section III-B, we have the following theorem.

Theorem 3: When a priori knowledge is unavailable, the EFIMs for the position and the orientation, using an N_a -antenna array, are given respectively by

$$\mathbf{J}_e^{\text{Array}}(\mathbf{p}) = \sum_{n \in \mathcal{N}_a} \mathbf{J}_e(\mathbf{p}_n^{\text{Array}}) - \frac{1}{\sum_{n \in \mathcal{N}_a} \sum_{k \in \mathcal{N}_b} \lambda_{nk} h_{nk}^2} \mathbf{q} \mathbf{q}^T, \quad (26)$$

and

$$\mathbf{J}_e^{\text{Array}}(\varphi) = \sum_{n \in \mathcal{N}_a} \sum_{k \in \mathcal{N}_b} \lambda_{nk} h_{nk}^2 - \mathbf{q}^T \left[\sum_{n \in \mathcal{N}_a} \mathbf{J}_e(\mathbf{p}_n^{\text{Array}}) \right]^{-1} \mathbf{q}, \quad (27)$$

where λ_{nk} is given by (73), $\mathbf{q}_{nk} = [\cos \phi_{nk} \quad \sin \phi_{nk}]^T$, and

$$\begin{aligned} \mathbf{J}_e(\mathbf{p}_n^{\text{Array}}) &= \sum_{k \in \mathcal{N}_b} \lambda_{nk} \mathbf{J}_r(\phi_{nk}), \\ \mathbf{q} &= \sum_{n \in \mathcal{N}_a} \sum_{k \in \mathcal{N}_b} \lambda_{nk} h_{nk} \mathbf{q}_{nk}, \end{aligned} \quad (28)$$

and

$$h_{nk} = \frac{d}{d\varphi} \Delta x_n(\mathbf{p}, \varphi) \cos \phi_{nk} + \frac{d}{d\varphi} \Delta y_n(\mathbf{p}, \varphi) \sin \phi_{nk}. \quad (29)$$

Proof: See Appendix D-A. \square

Corollary 4: The EFIM for the position is given by

$$\mathbf{J}_e^{\text{Array}}(\mathbf{p}) = \sum_{n \in \mathcal{N}_a} \mathbf{J}_e(\mathbf{p}_n^{\text{Array}}), \quad (30)$$

for orientation-aware localization.

Proof: (Outline) In orientation-aware localization, the angle φ is known and hence excluded from the parameter vector $\boldsymbol{\theta}$ in (25). Consequently, the proof of this corollary is analogous to that of Theorem 3 except that the components corresponding to φ are eliminated from the FIM in (69) and (70). One can obtain (30) after some algebra. \square

Remark 7: The EFIM $\mathbf{J}_e(\mathbf{p}_n^{\text{Array}})$ in (26) and (30) corresponds to the localization information from the n th antenna. We draw the following observation from the above theorem.

- The EFIM $\mathbf{J}_e^{\text{Array}}(\mathbf{p})$ in (26) consists of two parts: 1) the sum of localization information obtained by individual antennas, and 2) the information reduction due to the uncertainty in the orientation estimate, which is subtracted from the first part.²² Since $\mathbf{q}\mathbf{q}^T$ in the second part is a positive semi-definite 2×2 matrix and $\sum_{n \in \mathcal{N}_a} \sum_{k \in \mathcal{N}_b} \lambda_{nk} h_{nk}^2$ is always positive, we have the following inequality

$$\mathbf{J}_e^{\text{Array}}(\mathbf{p}) \preceq \sum_{n \in \mathcal{N}_a} \mathbf{J}_e(\mathbf{p}_n^{\text{Array}}). \quad (31)$$

The inequality implies that the EFIM for the position, using antenna arrays, is bounded above by the sum of all EFIMs corresponding to individual antennas, since the uncertainty in the orientation estimate degrades the localization accuracy, except for $\mathbf{q} = 0$ or orientation-aware localization (i.e., (30)).

- The EFIM $\mathbf{J}_e^{\text{Array}}(\mathbf{p})$ and $\mathbf{J}_e^{\text{Array}}(\varphi)$ depend only on the individual RI between each pair of anchors and antennas (through λ_{nk} 's and ϕ_{nk} 's), and the array geometry (through h_{nk} 's). Hence it is not necessary to *jointly* consider the received waveforms at the N_a antennas, implying that AOA obtained by antenna arrays does not

increase position accuracy. Though counterintuitive at first, this finding should not be too surprising since AOA is obtained indirectly by the antenna array through TOA measurements, whereas the TOA information has already been fully utilized for localization by individual antennas.

- The gain of using antenna arrays for localization mainly comes from the multiple copies of the waveform received at the N_a antennas (see (26)),²³ and its performance is similar to that of a single antenna with N_a measurements. The advantage of using antenna arrays lies in their ability of simultaneous measurements at the agent.

The equality in (31) is always achieved, independent of reference point, in orientation-aware localization. However, only a unique reference point achieves this equality in orientation-unaware localization. We define this unique point as the orientation center.

Definition 6 (Orientation Center): The orientation center is a reference point \mathbf{p}^* such that

$$\mathbf{J}_e^{\text{Array}}(\mathbf{p}^*) = \sum_{n \in \mathcal{N}_a} \mathbf{J}_e(\mathbf{p}_n^{\text{Array}}).$$

Proposition 3: Orientation center \mathbf{p}^* exists and is unique in orientation-unaware localization, and hence for any $\mathbf{p} \neq \mathbf{p}^*$,

$$\mathbf{J}_e^{\text{Array}}(\mathbf{p}) \prec \mathbf{J}_e^{\text{Array}}(\mathbf{p}^*).$$

Proof: See Appendix D-B. \square

Remark 8: The orientation center \mathbf{p}^* generally depends on the topology of the anchors and the agent, the properties of the received waveforms, the array geometry, and the array orientation. Since $\mathbf{q} = \mathbf{0}$ at the orientation center, the EFIMs for the array center and the orientation do not depend on each other, and hence the SPEB and SOEB can be calculated separately. The proposition also implies that the SPEB of reference points other than \mathbf{p}^* will be strictly larger than that of \mathbf{p}^* . The SPEB for any reference point is given in the next theorem.

Corollary 5: The SOEB $\mathcal{P}(\varphi)$ is independent of the reference point \mathbf{p} , and the SPEB is

$$\mathcal{P}(\mathbf{p}) = \mathcal{P}(\mathbf{p}^*) + \|\mathbf{p} - \mathbf{p}^*\|^2 \cdot \mathcal{P}(\varphi). \quad (32)$$

Proof: See Appendix D-C. \square

Remark 9: The SOEB does not depend on the specific reference point, which was not apparent in (27). However, this is intuitive since different reference points only introduce different translations, but not rotations. On the other hand, different reference point \mathbf{p} results in different h_{nk} 's and hence different \mathbf{q} , which in turn gives different EFIM for position (see (26)). We can interpret the relationship in (32) as follows: the SPEB of reference point \mathbf{p} is equal to that of the orientation center \mathbf{p}^* plus the orientation-induced position error, which is proportional to both the squared distance from \mathbf{p} to \mathbf{p}^* and the SOEB.

²²For notational convenience, we suppress the dependence of h_{nk} , λ_{nk} , and \mathbf{q} on the reference position \mathbf{p} .

²³In near-field scenarios where the antenna separation is on the order of the distances between the array and the anchors, additional gain that arises from the spatial diversity of the multiple antennas may be possible.

C. EFIM with A Priori Knowledge

We now consider a scenario in which the channel parameter vector κ_{nk} independent for different n 's and k 's. The independence assumption serve as a reasonable approximation of many realistic scenarios, especially near-field cases. When the different sets of channel parameters are correlated, our results provide an upper bound for the EFIM.

Proposition 4: When a priori knowledge of channel parameters is available and the set of channel parameters corresponding to different anchors and antennas are mutually independent, the RII λ_{nk} becomes (72).

Proof: See Appendix D-A. \square

We then consider the case where a priori knowledge of the agent's position and orientation is available in addition to channel knowledge. Note that the topology of the agent's antennas and anchors changes with the agent's positions and orientations. The expression of the EFIM can be derived analogous to (67), which is involved in general. Again to gain insights about the contribution of a priori position and orientation knowledge, we consider scenarios under condition

$$\mathbb{E}_{\mathbf{p}, \varphi} \{g(\mathbf{p}, \varphi)\} = g(\bar{\mathbf{p}}, \bar{\varphi}), \quad (33)$$

where $\bar{\varphi} = \mathbb{E}_{\varphi} \{\varphi\}$, for some functions $g(\cdot)$ involved in the derivation of the EFIM.

Corollary 6: When a priori position and orientation distribution of the agent satisfies (33), and the sets of channel parameters corresponding to different anchors and antennas are mutually independent, the EFIMs for the position and the orientation, using an N_a -antenna array, are given respectively by

$$\mathbf{J}_e^{\text{Array}}(\mathbf{p}) = \Xi_{\mathbf{p}} + \sum_{n \in \mathcal{N}_a} \sum_{k \in \mathcal{N}_b} \bar{\lambda}_{nk} \mathbf{J}_r(\bar{\phi}_{nk}) - \frac{1}{\sum_{n \in \mathcal{N}_a} \sum_{k \in \mathcal{N}_b} \bar{\lambda}_{nk} \bar{h}_{nk}^2 + \Xi_{\varphi}} \bar{\mathbf{q}} \bar{\mathbf{q}}^T,$$

and

$$J_e^{\text{Array}}(\varphi) = \Xi_{\varphi} + \sum_{n \in \mathcal{N}_a} \sum_{k \in \mathcal{N}_b} \bar{\lambda}_{nk} \bar{h}_{nk}^2 - \bar{\mathbf{q}}^T \left(\sum_{n \in \mathcal{N}_a} \sum_{k \in \mathcal{N}_b} \bar{\lambda}_{nk} \mathbf{J}_r(\bar{\phi}_{nk}) + \Xi_{\mathbf{p}} \right)^{-1} \bar{\mathbf{q}},$$

where $\bar{\lambda}_{nk}$, $\bar{\phi}_{nk}$, \bar{h}_{nk} and $\bar{\mathbf{q}}$ are corresponding functions in Theorem 3 of $\bar{\mathbf{p}}$ and $\bar{\varphi}$, respectively, and $\Xi_{\varphi} = \mathbf{F}_{\theta}(\varphi; \varphi, \varphi)$.

Proof: (Outline) The proof of this corollary is analogous to that of Theorem 3. Note that when condition (33) is satisfied, the a priori knowledge of position and orientation for localization can be characterized in the EFIM by using the approximation as in the proof of Proposition 2. \square

D. Discussions

1) *Far-field scenarios:* The antennas in the array are closely located in far-field scenarios, such that the received waveforms from each anchor experience statistically the same propagation channels. Hence we have $\phi_{nk} = \phi_k$ and $\lambda_{nk} = \lambda_k$ for all n , leading to $\mathbf{J}_e(\mathbf{p}_n^{\text{Array}}) = \mathbf{J}_e(\mathbf{p})$. We define an important reference point as follows.

Definition 7 (Array Center): The array center is defined as the position \mathbf{p}_0 , satisfying

$$\sum_{n \in \mathcal{N}_a} \Delta x_n(\mathbf{p}_0, \varphi) = 0 \quad \text{and} \quad \sum_{n \in \mathcal{N}_a} \Delta y_n(\mathbf{p}_0, \varphi) = 0.$$

Proposition 5: The array center becomes the orientation center in far-field scenarios.

Proof: See Appendix D-D. \square

Remark 10: Since the orientation center has the minimum SPEB, Proposition 5 implies that the array center always achieves the minimum SPEB in far-field scenarios. Hence the array center is a well-suited choice for the reference point, since its position can be determined from the array geometry alone, without requiring the received waveforms and the knowledge of the anchor's topology.

In far-field scenarios, we choose the array center \mathbf{p}_0 as the reference point. The results of Theorem 3 become

$$\mathbf{J}_e^{\text{Array}}(\mathbf{p}_0) = N_a \sum_{k \in \mathcal{N}_b} \lambda_k \mathbf{J}_r(\phi_k),$$

and

$$J_e^{\text{Array}}(\varphi) = \sum_{n \in \mathcal{N}_a} \sum_{k \in \mathcal{N}_b} \lambda_k \bar{h}_{nk}^2,$$

where \bar{h}_{nk} is a function of \mathbf{p}_0 . Similarly, when the a priori position and orientation knowledge is available and condition (33) is satisfied, the results of Proposition 6 become

$$\mathbf{J}_e^{\text{Array}}(\mathbf{p}_0) = N_a \sum_{k \in \mathcal{N}_b} \bar{\lambda}_k \mathbf{J}_r(\bar{\phi}_k) + \Xi_{\mathbf{p}},$$

and

$$J_e^{\text{Array}}(\varphi) = \sum_{n \in \mathcal{N}_a} \sum_{k \in \mathcal{N}_b} \bar{\lambda}_k \bar{h}_{nk}^2 + \Xi_{\varphi},$$

where \bar{h}_{nk} is a function of $\bar{\mathbf{p}}_0 = \mathbb{E}_{\mathbf{p}_0} \{\mathbf{p}_0\}$.

Note that the localization performance of an N_a -antenna array is equivalent to that of a single antenna with N_a measurements, regardless of the array geometry, in far-field scenarios.

2) *Multiple antennas at anchors:* When anchors are equipped with multiple antennas, each antenna can be viewed as an individual anchor. In this case, the agent's SPEB goes down with the number of the antennas at each anchor. Note that all the antennas of a given anchor provide RI approximately in the same direction with the same intensity, as they are closely located.

3) *Other related issues:* Other issues related to localization using wideband antenna arrays include the AOA estimation, the effect of multipath geometry, and the effect of array geometries. A more comprehensive performance analysis can be found in [11].

V. EFFECT OF CLOCK ASYNCHRONISM

In this section, we consider scenarios in which the clocks of all anchors are perfectly synchronized but the agent operates asynchronously with the anchors [68]. In such a scenario, the one-way time-of-flight measurement contains a time offset

between the agent's clock and the anchors' clock.²⁴ Here, we investigate the effect of the time offset on localization accuracy.

A. Localization with a Single Antenna

Consider the scenario described in Section II, where each agent is equipped with a single antenna. When the agent operates asynchronously with the anchors, the relationship of (2) becomes

$$\tau_k^{(l)} = \frac{1}{c} \left[\|\mathbf{p} - \mathbf{p}_k\| + b_k^{(l)} + B \right],$$

where B is a random parameter that characterizes the time offset in terms of distance, and the corresponding parameter vector $\boldsymbol{\theta}$ becomes

$$\boldsymbol{\theta} = \left[\mathbf{p}^T \quad B \quad \boldsymbol{\kappa}_1^T \quad \boldsymbol{\kappa}_2^T \quad \cdots \quad \boldsymbol{\kappa}_{N_b}^T \right]^T.$$

Similar to Theorem 2, where \mathbf{p} is deterministic but unknown and the remaining parameters are random, we have the following result.

Theorem 4: When a priori knowledge of the channel parameters and the time offset is available, and the sets of channel parameters corresponding to different anchors are mutually independent, the EFIMs for the position and the time offset are given respectively by

$$\mathbf{J}_e^B(\mathbf{p}) = \sum_{k \in \mathcal{N}_b} \lambda_k \mathbf{J}_r(\phi_k) - \frac{1}{\sum_{k \in \mathcal{N}_b} \lambda_k + \Xi_B} \mathbf{q}_B \mathbf{q}_B^T \quad (34)$$

and

$$J_e(B) = \sum_{k \in \mathcal{N}_b} \lambda_k + \Xi_B - \mathbf{q}_B^T \left(\sum_{k \in \mathcal{N}_b} \lambda_k \mathbf{J}_r(\phi_k) \right)^{-1} \mathbf{q}_B, \quad (35)$$

where λ_k is given by (65b), $\mathbf{q}_B = \sum_{k \in \mathcal{N}_b} \lambda_k \mathbf{q}_k$, and

$$\Xi_B \triangleq \mathbf{F}_\theta(B; B, B).$$

Proof: See Appendix E-A. \square

Remark 11: Since $\mathbf{q}_B \mathbf{q}_B^T$ is a positive semi-definite matrix and $\sum_{k \in \mathcal{N}_b} \lambda_k$ is positive in (34), compare to Theorem 2, we always have the inequality

$$\mathbf{J}_e^B(\mathbf{p}) \preceq \mathbf{J}_e(\mathbf{p}), \quad (36)$$

where the equality in (36) is achieved for time-offset-known localization (i.e., $\Xi_B = \infty$), or time-offset-independent localization (i.e., $\mathbf{q}_B = \mathbf{0}$). The former corresponds to the case where accurate knowledge of the time offset is available, while the latter depends on the RII from each anchor, and the topology of the anchors and agent. The inequality of (36)

²⁴We consider scenarios in which localization time is short relative to clock drifts, such that the time offset is the same for all measurements from the anchors.

results from the uncertainty in the additional parameter B , which degrades the localization accuracy. Hence the SPEB in the presence of uncertain time offset is always larger than or equal to that without a offset or with a known offset.

We next consider the case where a priori knowledge of the agent's position is available. When the a priori position distribution of the agent satisfies (22), we have the following corollary.

Corollary 7: When the a priori position distribution of the agent satisfies (22), and the sets of channel parameters corresponding to different anchors are mutually independent, the EFIMs for the position and the time offset are given respectively by

$$\mathbf{J}_e^B(\mathbf{p}) = \sum_{k \in \mathcal{N}_b} \bar{\lambda}_k \mathbf{J}_r(\bar{\phi}_k) + \Xi_B - \frac{1}{\sum_{k \in \mathcal{N}_b} \bar{\lambda}_k + \Xi_B} \bar{\mathbf{q}}_B \bar{\mathbf{q}}_B^T,$$

and

$$J_e(B) = \sum_{k \in \mathcal{N}_b} \bar{\lambda}_k + \Xi_B - \bar{\mathbf{q}}_B^T \left(\Xi_B + \sum_{k \in \mathcal{N}_b} \bar{\lambda}_k \mathbf{J}_r(\bar{\phi}_k) \right)^{-1} \bar{\mathbf{q}}_B,$$

where $\bar{\phi}_k$ is the angle from anchor k to $\bar{\mathbf{p}}$, $\bar{\lambda}_k$ is given by (68), and $\bar{\mathbf{q}}_B$ is a function of $\bar{\mathbf{p}}$.

Proof: (Outline) Conditions in (22) hold in far-field scenarios, and we can approximate the expectation over random parameter vector \mathbf{p} using the average position $\bar{\mathbf{p}}$. By following the steps of Theorem 4 and Proposition 2, we can derive the theorem after some algebra. \square

B. Localization with Antenna Arrays

Consider the scenario describing in Section IV where each agent is equipped with an array of N_a antennas. Incorporating the time offset B , (24) becomes

$$\tau_{nk}^{(l)} = \frac{1}{c} \left[\|\mathbf{p}_n^{\text{Array}} - \mathbf{p}_k\| + b_{nk}^{(l)} + B \right],$$

and the corresponding parameter vector $\boldsymbol{\theta}$ becomes

$$\boldsymbol{\theta} = \left[\mathbf{p}^T \quad \varphi \quad B \quad \boldsymbol{\kappa}_1^T \quad \boldsymbol{\kappa}_2^T \quad \cdots \quad \boldsymbol{\kappa}_N^T \right]^T.$$

Similar to Theorem 3, where \mathbf{p} and φ are deterministic but unknown and the remaining parameters are random, we have the following theorem.

Theorem 5: When a priori knowledge of the channel parameters is available, and the sets of channel parameters corresponding to different anchors and antennas are mutually independent, the EFIM for the position, the orientation, and the time offset, using an N_a -antenna array, is given by (37) shown at the bottom of the page, where $\Xi = \infty$ and $\Xi = 0$ correspond to orientation-aware and orientation-unaware localization, respectively, and λ_{nk} , \mathbf{q}_{nk} , and h_{nk} are given by (72), (28), and (29), respectively.

$$\mathbf{J}_e^{\text{Array-B}} = \begin{bmatrix} \sum_{n \in \mathcal{N}_a} \sum_{k \in \mathcal{N}_b} \lambda_{nk} \mathbf{q}_{nk} \mathbf{q}_{nk}^T & \sum_{n \in \mathcal{N}_a} \sum_{k \in \mathcal{N}_b} h_{nk} \lambda_{nk} \mathbf{q}_{nk} & \sum_{n \in \mathcal{N}_a} \sum_{k \in \mathcal{N}_b} \lambda_{nk} \mathbf{q}_{nk} \\ \sum_{n \in \mathcal{N}_a} \sum_{k \in \mathcal{N}_b} h_{nk} \lambda_{nk} \mathbf{q}_{nk}^T & \sum_{n \in \mathcal{N}_a} \sum_{k \in \mathcal{N}_b} h_{nk}^2 \lambda_{nk} + \Xi & \sum_{n \in \mathcal{N}_a} \sum_{k \in \mathcal{N}_b} h_{nk} \lambda_{nk} \\ \sum_{n \in \mathcal{N}_a} \sum_{k \in \mathcal{N}_b} \lambda_{nk} \mathbf{q}_{nk}^T & \sum_{n \in \mathcal{N}_a} \sum_{k \in \mathcal{N}_b} h_{nk} \lambda_{nk} & \sum_{n \in \mathcal{N}_a} \sum_{k \in \mathcal{N}_b} \lambda_{nk} + \Xi_B \end{bmatrix} \quad (37)$$

Proof: See Appendix E-B. \square

Remark 12: Theorem 5 gives the overall 4×4 EFIM for the position, the orientation, and the time offset, where individual EFIMs can be derived by applying the notion of EFI again.

We finally consider the case where a priori knowledge of the agent's position and orientation is available. The EFIM in far-field scenarios is given in the following corollary.

Corollary 8: When a priori knowledge of the agent's position, orientation, time-offset, and the channel parameters is available, and the sets of channel parameters corresponding to different anchors and antennas are mutually independent, in far-field scenarios, the EFIMs for the position, the orientation, and the time offset, using an N_a -antenna array, are given respectively by

$$\mathbf{J}_e^{\text{Array-B}}(\mathbf{p}_0) = N_a \sum_{k \in \mathcal{N}_b} \bar{\lambda}_k \mathbf{J}_r(\bar{\phi}_k) + \Xi_{\mathbf{p}} - \frac{1}{N_a \sum_{k \in \mathcal{N}_b} \bar{\lambda}_k + \Xi_B} \bar{\mathbf{q}}_B \bar{\mathbf{q}}_B^T,$$

$$J_e^{\text{Array-B}}(\varphi) = \sum_{n \in \mathcal{N}_a} \sum_{k \in \mathcal{N}_b} \bar{\lambda}_k \bar{h}_{nk}^2 + \Xi_{\varphi},$$

and

$$J_e^{\text{Array-B}}(B) = N_a \sum_{k \in \mathcal{N}_b} \bar{\lambda}_k + \Xi_B - \bar{\mathbf{q}}_B^T \left(N_a \sum_{k \in \mathcal{N}_b} \bar{\lambda}_k \mathbf{J}_r(\bar{\phi}_k) + \Xi_{\mathbf{p}} \right)^{-1} \bar{\mathbf{q}}_B,$$

where $\bar{\mathbf{p}}_0$ is the expected position of the agent's array center, $\bar{\phi}_k$ is the angle from anchor k to $\bar{\mathbf{p}}_0$, and $\bar{\lambda}_k$, $\bar{\mathbf{q}}_B$, and \bar{h}_{nk} are functions of $\bar{\mathbf{p}}_0$.

Proof: See Appendix E-C. \square

VI. DISCUSSIONS

In this section, we will provide discussions on some related issues in the paper. It includes 1) the relations of our results to the bounds based on signal metrics, 2) the achievability of the SPEB, and 3) generalization of the results to 3D localization.

A. Relation to Bounds Based on Signal Metrics

Analysis of localization performance in the literature mainly employs specific signal metrics, such as TOA, AOA, RSS, and TDOA, rather than utilizing the entire received waveforms. Our analysis is based on the received waveforms and exploits all the localization information inherent in these signal metrics, implicitly or explicitly. In particular, TOA and joint TOA/AOA metrics were incorporated in our analysis in Section III and IV, respectively. Similarly, TDOA and joint TDOA/AOA metrics were included in the analysis of Section V, and the RSS metric has been implicitly exploited from a priori channel knowledge in Section II-C2.

B. Achievability of the SPEB

Maximum a posterior (MAP) and maximum likelihood (ML) estimates respectively achieve the CRB asymptotically in the high SNR regimes for both the case with and without

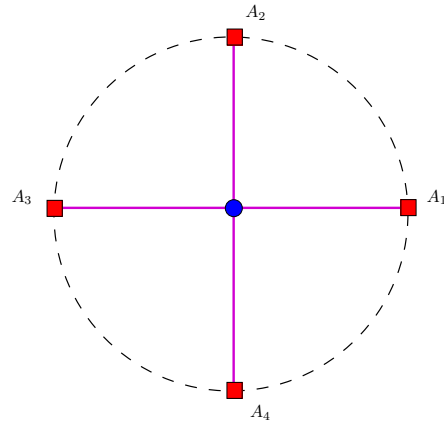


Fig. 4. Network topology: Four anchors are equally spaced on a circle with an agent at the center. All signals from the anchors to the agent are LOS.

a priori knowledge [50]. High SNR can be attained using sequences with good correlation properties [69]–[71], or simply repeated transmissions. Therefore, the SPEB is achievable.

C. Generalization to 3D Localization

All results obtained thus far can be easily extended to three-dimensional case, i.e., $\mathbf{p} = [x \ y \ z]^T$ and the RDM becomes

$$\mathbf{J}_r(\varphi_k, \phi_k) = \mathbf{q}_k \mathbf{q}_k^T,$$

where φ_k and ϕ_k are the angles in the coordinates, and

$$\mathbf{q}_k = [\cos \varphi_k \cos \phi_k \quad \sin \varphi_k \cos \phi_k \quad \sin \phi_k]^T.$$

Similarly, we can obtain a corresponding 3×3 EFIM in the form of (21).

VII. NUMERICAL RESULTS

In this section, we illustrate applications of our analytical results using numerical examples. We deliberately restrict our attention to a simple network to gain insights, although our analytical results are valid for arbitrary topology with any number of anchors and any number of MPCs in the received waveforms.

A. Effect of Path-Overlap

We first investigate the effect of path-overlap on the SPEB when a priori knowledge is unavailable. In particular, we compare the SPEB obtained by the *full-parameter model* proposed in this paper and that obtained by the *partial-parameter model* proposed in [28]. In the partial-parameter model, the amplitudes of MPCs are assumed to be known and hence excluded from the parameter vector.

Consider a simple network with four anchors ($N_b = 4$) equally spaced on a circle and an agent at the center receiving all LOS signals (see Fig. 4). Each waveform consists of two paths: one LOS path ($\text{SNR}_k^{(1)} = 0$ dB) and one NLOS path ($\text{SNR}_k^{(2)} = -3$ dB), and the separations of the two paths $\tau_k^{(2)} - \tau_k^{(1)}$ are identical for all k . In addition, the transmitted waveform is a second derivative of Gaussian pulse with width

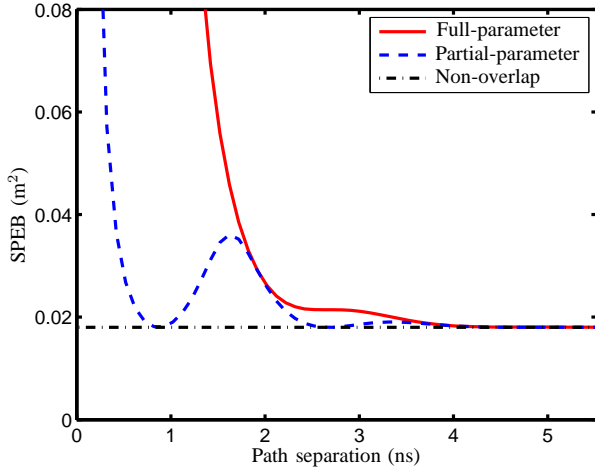


Fig. 5. SPEB as a function of path separation for the full-parameter, partial-parameter, and non-overlap models, without a priori knowledge.

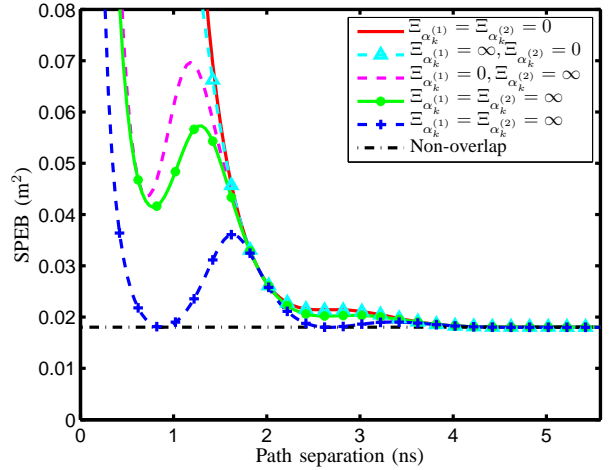
approximately equal to 4 ns. Figure 5 shows the SPEB as a function of path separation $\tau_k^{(2)} - \tau_k^{(1)}$ according to Theorem 1.

We can draw the following observations. First of all, path-overlap increases the SPEB in both models, since it reduces the ability to estimate the first path and hence decreases the RII. Note that the shape of the curves depends on the autocorrelation function of the waveform $s(t)$ [47]. Secondly, when the path separation exceeds the pulse width (approximately 4 ns), the two models give the same SPEB, which equals the non-overlapping case. In such cases, the first contiguous-cluster contains only the first path, and hence the RII is determined by the first paths. This agrees with the analysis in Section III. Thirdly, excluding the amplitudes from the parameter vector incorrectly provides more RI when the two paths overlap, and hence the partial-parameter model results in a loose bound. This demonstrates the importance of using the full-parameter model.

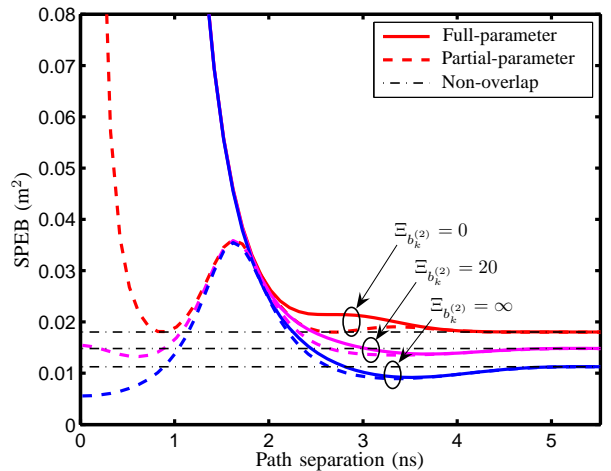
B. Improvement from A Priori Channel Knowledge

We then quantify the contribution of the a priori knowledge of channel parameters to the SPEB. The network topology and channel parameters are the same as those in Section VII-A, except a priori knowledge of $\alpha_k^{(1)}$, $\alpha_k^{(2)}$ and $b_k^{(2)}$ is now available. For simplicity, we consider these parameters to be independent a priori and denote the a priori Fisher information of parameter θ_1 by $\Xi_{\theta_1} = \mathbf{F}_{\theta}(\theta; \theta_1, \theta_1)$. In Fig. 6(a), the SPEBs are plotted as functions of the path separation for different a priori knowledge of $\alpha_k^{(1)}$ and $\alpha_k^{(2)}$ (no a priori knowledge of $b_k^{(2)}$); while in Fig. 6(b), the SPEBs are plotted for different a priori knowledge of $b_k^{(2)}$ (no a priori knowledge of $\alpha_k^{(1)}$ and $\alpha_k^{(2)}$).

We have the following observations. First of all, the SPEB decreases with the a priori knowledge of the amplitudes and the NLOS biases. This should be expected since a priori channel knowledge increases the RII and thus localization



(a) SPEB with a priori knowledge of $\alpha_k^{(1)}$ and $\alpha_k^{(2)}$, while $\Xi_{b_k^{(2)}} = 0$.



(b) SPEB with a priori knowledge of $b_k^{(2)}$, while $\Xi_{\alpha_k^{(1)}} = \Xi_{\alpha_k^{(2)}} = 0$.

Fig. 6. SPEB with a priori knowledge of the amplitudes and the NLOS biases as a function of path separation, respectively.

accuracy, as indicated in Corollary 2. Moreover, the NLOS components are shown to be beneficial for localization in the presence of a priori biases knowledge, as proven in Section III-B. Secondly, as the a priori knowledge of the amplitudes approaches infinity, the SPEB in Fig. 6(a) obtained using the full-parameter model converges to that in Fig. 5 obtained using the partial-parameter model. This is because the partial-parameter model excludes the amplitudes from the parameter vector, which is equivalent to assuming known amplitudes and hence infinite a priori Fisher information for the amplitudes ($\Xi_{\alpha_k^{(1)}} = \Xi_{\alpha_k^{(2)}} = \infty$). Thirdly, it is surprising to observe that, when the a priori knowledge of the NLOS biases is available, path-overlap can result in a lower SPEB compared to non-overlapping scenarios. This occurs at certain regions of path separations, depending on the autocorrelation function of $s(t)$. Intuitively, path-overlap can lead to a higher SNR compared to non-overlapping cases, when a priori knowledge of the NLOS

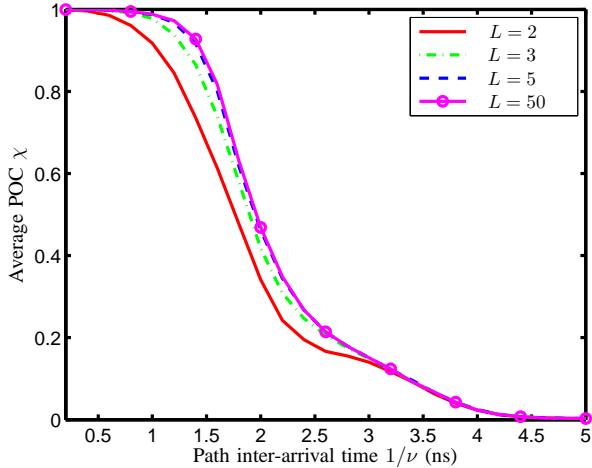


Fig. 7. POC as a function of the path inter-arrival time for different number of MPCs.

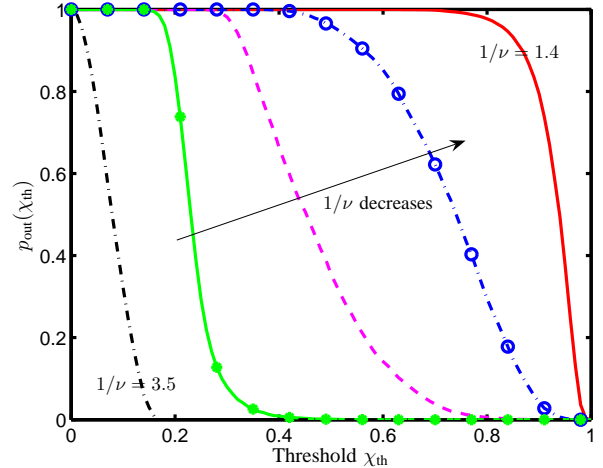


Fig. 8. RAO as a function of the threshold χ_{th} for different path inter-arrival time $1/\nu$ with $L = 50$. The five curves correspond to inter-arrival time $1/\nu = 3.5, 2.5, 2, 1.6, 1.4$ ns, respectively.

biases is available.

C. Path-Overlap Coefficient

We now investigate the dependence of POC χ on path arrival rate. We first generate channels with L MPCs according to a simple Poisson model with a fixed arrival rate ν , and then calculate χ according to (61). Figure 7 shows the average path-overlap coefficient as a function of path inter-arrival rate ($1/\nu$) for different number of MPCs, where the averaging is obtained by Monte-Carlo simulations.

We have the following observations. First of all, the POC χ is monotonically decreasing from 1 to 0 with $1/\nu$. This agrees with our intuition that denser multipath propagation causes more interference between the first path and other MPCs, and hence the received waveform provides less RII. Secondly, for a fixed ν , the POC increases with L . This should be expected as additional MPCs may interfere with earlier paths, which degrades the estimation accuracy of the first path and thus reduces the RII. Thirdly, observe that beyond $L = 5$ paths, χ does not increase significantly. This indicates that the effect of additional MPCs beyond the fifth path do not contribute to the RII, regardless of the power dispersion profile of the received waveforms.

D. Outage in Ranging Ability

We have observed that the channel quality for ranging is characterized by the POC. If the multipath propagation has a larger POC (close to 1), we may consider the channel in outage for ranging. We define the ranging ability outage (RAO) as

$$p_{\text{out}}(\chi_{\text{th}}) \triangleq \mathbb{P}\{\chi > \chi_{\text{th}}\},$$

where χ_{th} is the threshold for the POC. The RAO tells us that with probability $p_{\text{out}}(\chi_{\text{th}})$, the propagation channel is unsatisfactory for ranging.

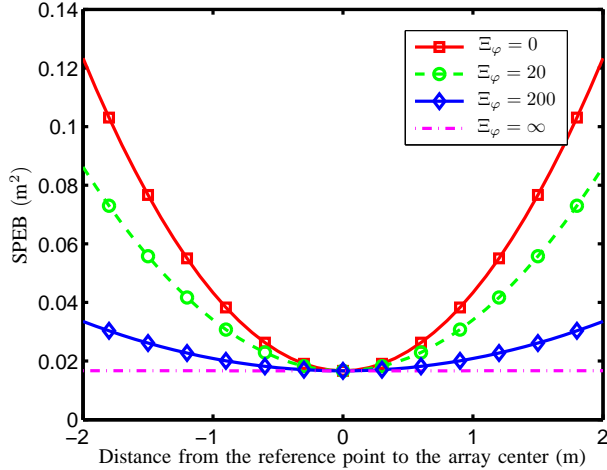
The RAO as a function of χ_{th} for different Poisson arrival rate is plotted in Fig. 8 for a channel with $L = 50$. The RAO

decreases from 1 to 0, as the threshold χ_{th} increases or the path arrival rate ν decreases. This should be expected because the probability of path-overlap decreases with the path arrival rate, and consequently decreases the RAO. The RAO can be used as a measure to quantify the channel quality for ranging and to guide the design of the optimal transmitted waveform for ranging.

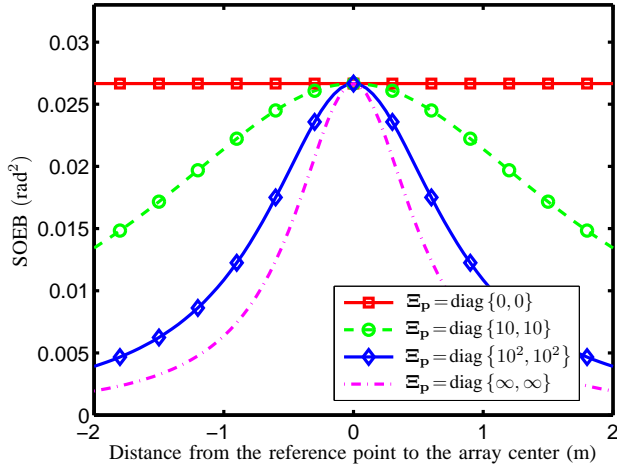
E. SPEB and SOEB for Wideband Antenna Array Systems

We consider the SPEB and SOEB for different reference points of a uniform linear array (ULA). The numerical results are based on a network with six equally spaced anchor nodes ($N_b = 6$) located on a circle with an agent in the center. The agent is equipped with a 4-antenna array ($N_a = 4$) whose spacing is 0.5 m. In far-field scenarios, $\lambda_{nk} = \lambda_k = 10$ and $\phi_{nk} = \phi_k$. Fig. 9(a) and Fig. 9(b) show the SPEB and SOEB, respectively, as a function of different reference point along the ULA for different a priori knowledge of the orientation and reference point.

We have the following observations. First of all, a priori knowledge of the orientation improves the localization accuracy as the SPEB decreases with Ξ_φ . The curves for $\Xi_\varphi = 0$ and $\Xi_\varphi = \infty$ correspond to the orientation-unaware and orientation-aware cases, respectively. As a counterpart, a priori knowledge of the reference point improves the orientation accuracy as the SOEB decreases with Ξ_p . This agrees with both intuition and Theorem 3. Secondly, the array center has the best localization accuracy, and its SPEB does not depend on Ξ_φ , which agrees with Theorem 3. On the other hand, the array center exhibits the worst orientation accuracy, and its SOEB does not depend on Ξ_p . This should be expected since the knowledge for the array center tells nothing about the array orientation. Thirdly, the SPEB increases with both the distance from the reference point to the array center and the SOEB, as predicted by Corollary 5. On the contrary, the SOEB decreases



(a) SPEB as a function of the reference point-to-array center distance



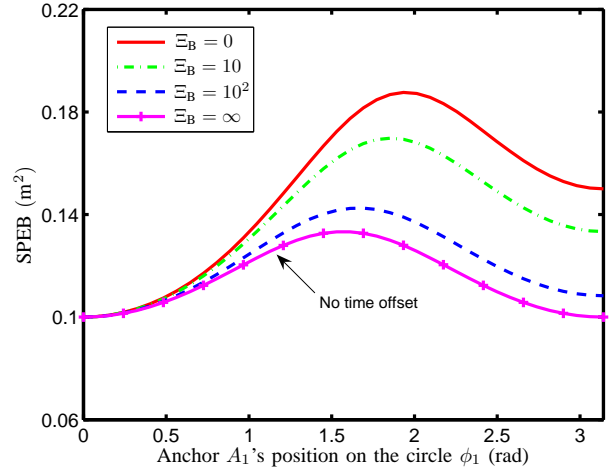
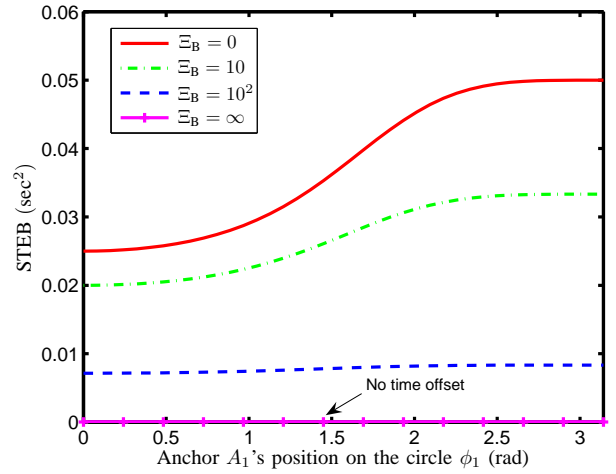
(b) SOEB as a function of the reference point-to-array center distance

Fig. 9. SPEB and SOEB with different a priori knowledge of agent's position and orientation, respectively

as a function of the distance from the reference point to the array center if a priori knowledge of the reference point is available. This observation can be verified by Theorem 3. Last but not least, the SPEB is independent of specific reference point if $\Xi_\varphi = \infty$, as referred to orientation-aware localization, and the SOEB is independent of the specific reference point if $\Xi_p = \mathbf{0}$, as shown in Corollary 5.

F. SPEB with Time Offset and Squared Timing Error Bound

We finally investigate the effect of time offset on the SPEB and squared timing error bound (STEB) for the network illustrated in Fig. 4. The RII from each anchor $\lambda_k = 10$, $k \in \{1, 2, 3, 4\}$. Initially, four anchors are placed at $\phi_1 = 0$, $\phi_2 = \pi/2$, $\phi_3 = \pi$, and $\phi_4 = 3\pi/2$, respectively. We then vary the position of Anchor A_1 counter-clockwise along the circle. Figure 10(a) and 10(b) show the SPEB and STEB, respectively, as functions of ϕ_1 for different a priori knowledge of the time offset.

(a) SPEB as a function of Anchor A_1 's position(b) STEB as a function of Anchor A_1 's positionFig. 10. SPEB and STEB with different a priori knowledge of the time offset, and $\Xi_B = 0, 10, 10^2, \infty$ respectively.

We have the following observations. First of all, both the SPEB and STEB decrease with the a priori knowledge of the time offset. The SPEB for the case $\Xi_B = \infty$ in Fig. 10(a), i.e., known time offset, is equal to that of a system without a time offset. On the other hand, when $\Xi_B = \infty$, the STEB in Fig. 10(b) is equal to zero regardless of ϕ_1 since the offset is completely known. Secondly, all the curves in Fig. 10(a) have the same value at $\phi_1 = 0$. The time offset has no effect on the SPEB at this point, since $\mathbf{q}_B = \mathbf{0}$, referred to as *time-offset-independent* localization. In this case, both the SPEB and STEB achieve their minimum, implying that location and timing information of a network are closely related. Third, as ϕ_1 increases from 0 to π , all the curves in Fig. 10(a) first increase and then decrease, whereas all the curves in Fig. 10(b) increase monotonically. We give the following interpretations: the estimation error of time offset in Fig. 10(b) becomes larger when all the anchors tend to gather on one side of the agent (ϕ_1 increases from 0 to π). In Fig. 10(a), the SPEB first increases

since both the localization information $\sum_{k \in \mathcal{N}_b} \lambda_k \mathbf{J}_r(\phi_k)$ in (34) and the information for the time offset becomes smaller. Then the SPEB decreases since the localization information increases (when $\phi_1 > \pi/2$) faster compared to the decrease of the information for time offset. Note in Fig. 10(a) that although $\phi_1 = 0$ and $\phi_1 = \pi$ result in the same SPEB in the absence of time offset, $\phi_1 = 0$ gives a better performance in the presence of time offset.

VIII. CONCLUSION

In this paper, we developed a framework to study wideband wireless location-aware networks and determined their localization accuracy. In particular, we characterized the localization accuracy in terms of a performance measure called the squared position error bound (SPEB), and derived the SPEB by applying the notion of equivalent Fisher information. This methodology provides insights into the essence of the localization problem by unifying the localization information from the a priori knowledge of the agent's position and information from individual anchors. We showed that the contributions from anchors, incorporating both measurements and a priori channel knowledge, can be expressed in a canonical form as a weighted sum of the ranging direction matrix. Our results are derived from the received waveforms themselves rather than the signal metrics extracted from the waveforms. Therefore, our framework exploits all the information inherent in the received waveforms, and consequently the results in this paper serve as fundamental limits of localization accuracy. These results can be used as guidelines for localization system design, as well as benchmarks for location-aware networks.

APPENDIX A

FISHER INFORMATION MATRIX DERIVATION

To facilitate the analysis, we consider a mapping from $\boldsymbol{\theta}$ into another parameter vector $\boldsymbol{\eta} = [\boldsymbol{\eta}_1^T \ \boldsymbol{\eta}_2^T \ \cdots \ \boldsymbol{\eta}_{N_b}^T]^T$, where $\boldsymbol{\eta}_k = [\tau_k^{(1)} \ \tilde{\alpha}_k^{(1)} \ \cdots \ \tau_k^{(L_k)} \ \tilde{\alpha}_k^{(L_k)}]^T$ with $\tilde{\alpha}_k^{(l)} \triangleq \alpha_k^{(l)}/c$. When the agent is localizable,²⁵ this mapping is a bijection and provides an alternative expression for the FIM as

$$\mathbf{J}_\theta = \mathbf{T} \mathbf{J}_\eta \mathbf{T}^T, \quad (38)$$

where \mathbf{J}_η is the FIM for $\boldsymbol{\eta}$, and \mathbf{T} is the Jacobian matrix for the transformation from $\boldsymbol{\theta}$ to $\boldsymbol{\eta}$, given respectively by

$$\mathbf{J}_\eta \triangleq \mathbf{F}_r(\mathbf{r}|\boldsymbol{\theta}; \boldsymbol{\eta}, \boldsymbol{\eta}) = \begin{bmatrix} \boldsymbol{\Lambda}_L & \mathbf{0} \\ \mathbf{0} & \boldsymbol{\Lambda}_{NL} \end{bmatrix}, \quad (39)$$

and

$$\mathbf{T} \triangleq \frac{\partial \boldsymbol{\eta}}{\partial \boldsymbol{\theta}} = \frac{1}{c} \begin{bmatrix} \mathbf{T}_L & \mathbf{T}_{NL} \\ \mathbf{0} & \mathbf{I} \end{bmatrix}, \quad (40)$$

with $\mathbf{0}$ denoting a matrix of all zeros and \mathbf{I} denoting an identity matrix. The block matrices \mathbf{T}_L , \mathbf{T}_{NL} , $\boldsymbol{\Lambda}_L$, and $\boldsymbol{\Lambda}_{NL}$ are given

as follows:

$$\begin{aligned} \mathbf{T}_L &= \begin{bmatrix} \mathbf{G}_1 & \mathbf{G}_2 & \cdots & \mathbf{G}_M \\ \mathbf{D}_1 & & & \mathbf{0} \\ & \mathbf{D}_2 & & \\ & & \ddots & \\ \mathbf{0} & & & \mathbf{D}_M \end{bmatrix}, \\ \mathbf{T}_{NL} &= \begin{bmatrix} \mathbf{G}_{M+1} & \cdots & \mathbf{G}_{N_b} \\ \mathbf{0} & \cdots & \mathbf{0} \end{bmatrix}, \\ \boldsymbol{\Lambda}_L &= \text{diag} \{ \boldsymbol{\Psi}_1, \boldsymbol{\Psi}_2, \dots, \boldsymbol{\Psi}_M \}, \end{aligned} \quad (41)$$

and

$$\boldsymbol{\Lambda}_{NL} = \text{diag} \{ \boldsymbol{\Psi}_{M+1}, \boldsymbol{\Psi}_{M+2}, \dots, \boldsymbol{\Psi}_{N_b} \}, \quad (42)$$

where $\mathbf{D}_k = [\mathbf{0} \ \mathbf{I}_{2L_k-1}]$,

$$\mathbf{G}_k = \mathbf{q}_k \mathbf{1}_k^T \quad \text{with} \quad \mathbf{1}_k = \underbrace{[1 \ 0 \ \cdots \ 1 \ 0]^T}_{2L_k \text{ components}}, \quad (43)$$

$\mathbf{q}_k = [\cos \phi_k \ \sin \phi_k]^T$, and $\boldsymbol{\Psi}_k \in \mathbb{R}^{2L_k \times 2L_k}$ is given by

$$\boldsymbol{\Psi}_k \triangleq \mathbf{F}_r(\mathbf{r}|\boldsymbol{\theta}; \boldsymbol{\eta}_k, \boldsymbol{\eta}_k). \quad (44)$$

Note that elements in $\boldsymbol{\Psi}_k$ can be expressed as

$$\begin{aligned} \mathbb{E}_r \left\{ -\frac{\partial^2 \ln f(\mathbf{r}|\boldsymbol{\theta})}{\partial \tau_k^{(i)} \partial \tau_k^{(j)}} \right\} &= \frac{2\alpha_k^{(i)} \alpha_k^{(j)}}{N_0} \int |2\pi f S(f)|^2 \exp \left\{ -j2\pi f (\tau_k^{(i)} - \tau_k^{(j)}) \right\} df \\ &= \frac{2\alpha_k^{(i)} \alpha_k^{(j)}}{N_0} \frac{\partial^2}{\partial \tau_k^{(i)} \partial \tau_k^{(j)}} R_s \left(\tau_k^{(i)} - \tau_k^{(j)} \right), \end{aligned}$$

$$\begin{aligned} \mathbb{E}_r \left\{ -\frac{\partial^2 \ln f(\mathbf{r}|\boldsymbol{\theta})}{\partial \tau_k^{(i)} \partial \tilde{\alpha}_k^{(j)}} \right\} &= \frac{2\alpha_k^{(i)} c}{N_0} \int j2\pi f |S(f)|^2 \exp \left\{ -j2\pi f (\tau_k^{(i)} - \tau_k^{(j)}) \right\} df \\ &= \frac{2\alpha_k^{(i)} c}{N_0} \frac{\partial}{\partial \tau_k^{(i)}} R_s \left(\tau_k^{(i)} - \tau_k^{(j)} \right), \end{aligned}$$

and

$$\begin{aligned} \mathbb{E}_r \left\{ -\frac{\partial^2 \ln f(\mathbf{r}|\boldsymbol{\theta})}{\partial \tilde{\alpha}_k^{(i)} \partial \tilde{\alpha}_k^{(j)}} \right\} &= \frac{2c^2}{N_0} \int |S(f)|^2 \exp \left\{ -j2\pi f (\tau_k^{(i)} - \tau_k^{(j)}) \right\} df \\ &= \frac{2c^2}{N_0} R_s \left(\tau_k^{(i)} - \tau_k^{(j)} \right), \end{aligned}$$

where $R_s(\tau) = \int s(t)s(t-\tau)dt$. In particular,

$$[\boldsymbol{\Psi}_k]_{1,1} = \mathbf{F}_r(\mathbf{r}|\boldsymbol{\theta}; \tau_k^{(1)}, \tau_k^{(1)}) = 8\pi^2 \beta^2 \text{SNR}_k^{(1)}, \quad (46)$$

where β and $\text{SNR}_k^{(i)}$ are given by (17) and (18), respectively. Substituting (39) and (40) into (38), we have the FIM \mathbf{J}_θ in (7).

²⁵Note that an agent is said to be localizable if its position can be determined by the signal metrics extracted from the waveforms received from neighboring anchors, i.e., triangulation is possible. This is true when $M \geq 3$, or in some special cases when $M = 2$.

APPENDIX B

WIDEBAND CHANNEL MODEL AND A PRIORI CHANNEL KNOWLEDGE

Wideband channel measurements have shown that MPCs follow random arrival and their amplitudes are subject to path loss, large and small-scale fading. While our discussion is valid for any wideband channels described by (1), we consider the model of IEEE 802.15.4a standard for exposition. Specifically, this standard uses Poisson arrivals, log-normal shadowing, Nakagami small-scale fading with exponential power dispersion profile (PDP) [26].

A. Path Arrival Time

The arrival time of MPCs is commonly modeled by a Poisson process [26], [64]. Given the path arrival rate ν , we have

$$g_{\tau_k}(\tau_k^{(l)} | \tau_k^{(l-1)}) = \nu \exp\left\{-\nu(\tau_k^{(l)} - \tau_k^{(l-1)})\right\},$$

for $\tau_k^{(l)} \geq \tau_k^{(l-1)}$ and $l \geq 2$. Using (2), we obtain

$$g_{b_k}(b_k^{(l)} | b_k^{(l-1)}) = \frac{\nu}{c} \exp\left\{-\frac{\nu}{c}(b_k^{(l)} - b_k^{(l-1)})\right\}, \quad (47)$$

for $b_k^{(l)} \geq b_k^{(l-1)}$ and $l \geq 1$. Note that we let $b_k^{(0)} = 0$ for consistency.

B. Path Loss and Large-Scale Fading

The RSS in dB at the distance d_k can be written as [26]

$$P_k = P_0 - 10\varrho \log_{10}\left(\frac{d_k}{d_0}\right) + w,$$

where P_0 is the expected RSS at the reference distance d_0 , ϱ is the propagation (path gain) exponent, and w is a random variable (r.v.) that accounts for large-scale fading, or shadowing. Shadowing is usually modeled with a log-normal distribution, such that w is a Gaussian r.v. with zero-mean and variance σ_S^2 , i.e., $w \sim N(0, \sigma_S^2)$.²⁶ The PDF of the RSS of $r_k(t)$ can then be written as

$$g_P(P_k | d_k) \propto \exp\left\{-\frac{1}{2\sigma_S^2}\left[P_k - P_0 + 10\varrho \log_{10}\left(\frac{d_k}{d_0}\right)\right]^2\right\}, \quad (48)$$

where $d_k = \|\mathbf{p} - \mathbf{p}_k\|$, and P_k is given by

$$P_k = 10 \log_{10} \left[\sum_{l=1}^{L_k} \mathbb{E}_s \left\{ \left| \alpha_k^{(l)} \right|^2 \right\} \right],$$

with $\mathbb{E}_s \{\cdot\}$ denoting the average over small-scale fading.

²⁶The standard deviation is typically 1-2 dB (LOS) and 2-6 dB (NLOS) [21] around the path gain.

C. Power Dispersion Profile and Small-Scale Fading

As in [24], [26], we consider an exponential PDP given by,²⁷

$$\mathbb{E}_s \left\{ \left| \alpha_k^{(l)} \right|^2 \right\} = Q_k \exp\left(-\frac{\tau_k^{(l)}}{\gamma_k}\right) \triangleq Q_k^{(l)}, \quad (49)$$

where γ_k is the decay constant, and Q_k is a normalization coefficient such that

$$Q_k = \frac{10^{P_k/10}}{\sum_{l=0}^{L_k} \exp\left(-\tau_k^{(l)}/\gamma_k\right)}. \quad (50)$$

In addition, $\alpha_k^{(l)}$ is a Nakagami r.v. with second moment given by (49). Specifically, we have

$$\begin{aligned} g_{\alpha_k}(\alpha_k^{(l)} | \mathbf{b}_k, d_k, P_k) &= g_{\alpha_k}(\alpha_k^{(l)} | \tau_k, P_k) \\ &= \frac{2}{\Gamma(m_l)} \left(\frac{m_l}{Q_k^{(l)}}\right)^{m_l} \left| \alpha_k^{(l)} \right|^{2m_l-1} \exp\left(-\frac{m_l}{Q_k^{(l)}} \left| \alpha_k^{(l)} \right|^2\right), \end{aligned} \quad (51)$$

where $\Gamma(m_l)$ is the gamma function and $m_l \geq 1/2$ is the Nakagami m -factor, which is a function of τ_k [26].

D. A Priori PDF for Multipath Parameters

The joint PDF of the multipath parameters and the RSS, conditioned on the distance from anchor k to the agent, can be derived as

$$\begin{aligned} f(\alpha_k, \mathbf{b}_k, P_k | d_k) &= g_P(P_k | d_k) \prod_{l=1}^{L_k} g_{\alpha_k}(\alpha_k^{(l)} | \mathbf{b}_k, d_k, P_k) \\ &\quad \times \prod_{l=1}^{L_k} g_{b_k}(b_k^{(l)} | b_k^{(l-1)}). \end{aligned} \quad (52)$$

By integrating over P_k , we obtain the PDF of the multipath parameters of $r_k(t)$ as follows

$$\begin{aligned} f(\boldsymbol{\kappa}_k | d_k) &= f(\alpha_k, \mathbf{b}_k | d_k) \\ &= \int_{-\infty}^{\infty} f(\alpha_k, \mathbf{b}_k, P_k | d_k) dP_k. \end{aligned} \quad (53)$$

Equation (53) characterizes the a priori knowledge of channel parameters, and can be obtained, for IEEE 802.15.4a standard, by substituting (47), (48) and (51) into (52) and (53). Note that since \mathbf{p}_k is known, d_k is a function of \mathbf{p} and hence we have (9).

APPENDIX C

PROOFS OF THE RESULTS IN SECTION III

A. Proof of Theorem 1

Proof: We first prove that $\mathbf{J}_e(\mathbf{p})$ is given by (15). We partition \mathbf{G}_k in (43) and $\mathbf{\Psi}_k$ in (44) as

$$\mathbf{G}_k \triangleq \begin{bmatrix} \mathbf{q}_k & \check{\mathbf{G}}_k \end{bmatrix} \quad \text{and} \quad \mathbf{\Psi}_k = \begin{bmatrix} 8\pi^2\beta^2 \text{SNR}_k^{(1)} & \mathbf{k}_k^T \\ \mathbf{k}_k & \check{\mathbf{\Psi}}_k \end{bmatrix},$$

²⁷Note that the first component of LOS signals can exhibit a stronger strength than (49) in some UWB measurement [72]. In such cases, (49) and (50) need to be modified, accordingly.

where $[\Psi_k]_{1,1}$ is obtained by (46), $\mathbf{k}_k \in \mathbb{R}^{2L_k-1}$, $\check{\Psi}_k \in \mathbb{R}^{(2L_k-1) \times (2L_k-1)}$, and

$$\check{\mathbf{G}}_k = \mathbf{q}_k \underbrace{\begin{bmatrix} 0 & 1 & 0 & \cdots & 1 & 0 \end{bmatrix}^T}_{2L_k-1 \text{ components}}.$$

Using these notations, we can write the EFIM given by (14) in Proposition 1, after some algebra, in the form of (12),

$$\mathbf{A} \triangleq 8\pi^2\beta^2 \sum_{k \in \mathcal{N}_L} \text{SNR}_k^{(1)} \mathbf{q}_k \mathbf{q}_k^T + \sum_{k \in \mathcal{N}_L} \left\{ \check{\mathbf{G}}_k \mathbf{k}_k \mathbf{q}_k^T + \mathbf{q}_k \mathbf{k}_k^T \check{\mathbf{G}}_k^T + \check{\mathbf{G}}_k \check{\Psi}_k \check{\mathbf{G}}_k^T \right\},$$

$$\mathbf{B} \triangleq \begin{bmatrix} \mathbf{q}_1 \mathbf{k}_1^T + \check{\mathbf{G}}_1 \check{\Psi}_1 & \cdots & \mathbf{q}_M \mathbf{k}_M^T + \check{\mathbf{G}}_M \check{\Psi}_M \end{bmatrix},$$

and

$$\mathbf{C} \triangleq \text{diag} \left\{ \check{\Psi}_1, \check{\Psi}_2, \dots, \check{\Psi}_M \right\}.$$

Applying the notion of EFI as in (13), we obtain the 2×2 $\mathbf{J}_e(\mathbf{p})$ as

$$\mathbf{J}_e(\mathbf{p}) = \frac{8\pi^2\beta^2}{c^2} \sum_{k \in \mathcal{N}_L} (1 - \chi_k) \text{SNR}_k^{(1)} \mathbf{q}_k \mathbf{q}_k^T, \quad (55)$$

where the POC

$$\chi_k \triangleq \frac{\mathbf{k}_k^T \check{\Psi}_k^{-1} \mathbf{k}_k}{8\pi^2\beta^2 \text{SNR}_k^{(1)}}. \quad (56)$$

This completes the proof of (15).

Next, we show that only the first contiguous-cluster contains information for localization. Let us focus on χ_k . Define the following notations for convenience:

$$R_s(i, j) \triangleq R_s(t)|_{t=\tau_k^{(i)} - \tau_k^{(j)}},$$

$$\ddot{R}_s(i, j) \triangleq -\frac{\partial^2}{\partial t^2} R_s(t)|_{t=\tau_k^{(i)} - \tau_k^{(j)}},$$

and

$$\dot{R}_s(i, j) \triangleq \frac{\partial}{\partial t} R_s(t)|_{t=\tau_k^{(i)} - \tau_k^{(j)}} = -\dot{R}_s(j, i).$$

If the length of the first contiguous-cluster in the received waveform is \tilde{L}_k where $1 \leq \tilde{L}_k \leq L_k$, then $\ddot{R}_s(i, j) = \dot{R}_s(i, j) = R_s(i, j) = 0$ for $i \in \{1, 2, \dots, \tilde{L}_k\}$ and $j \in \{\tilde{L}_k + 1, \tilde{L}_k + 2, \dots, L_k\}$, and²⁸

$$\mathbf{k}_k \triangleq \begin{bmatrix} \tilde{\mathbf{k}}_k^T & \mathbf{0}^T \end{bmatrix}^T \quad \text{and} \quad \check{\Psi}_k \triangleq \begin{bmatrix} \check{\Psi}_k & \mathbf{0} \\ \mathbf{0} & \boxtimes \end{bmatrix},$$

²⁸ \boxtimes is a block matrix that is irrelevant to the rest of the derivation.

where $\tilde{\mathbf{k}}_k \in \mathbb{R}^{2\tilde{L}_k-1}$ and $\check{\Psi}_k \in \mathbb{R}^{(2\tilde{L}_k-1) \times (2\tilde{L}_k-1)}$. Hence (56) becomes

$$\chi_k = \frac{\tilde{\mathbf{k}}_k^T \check{\Psi}_k^{-1} \tilde{\mathbf{k}}_k}{8\pi^2\beta^2 \text{SNR}_k^{(1)}}, \quad (57)$$

which depends only on the first \tilde{L}_k paths, implying that only the first contiguous-cluster of LOS signals contains information for localization.

Finally, we show that χ_k is independent of $\alpha_k^{(l)}$. Note that $\check{\Psi}_k$ and \mathbf{k}_k can be written as

$$\check{\Psi}_k = \frac{2}{N_0} \text{diag} \left\{ c, \alpha_k^{(2)}, c, \dots, \alpha_k^{(L_k)}, c \right\} \Upsilon_k \times \text{diag} \left\{ c, \alpha_k^{(2)}, c, \dots, \alpha_k^{(L_k)}, c \right\}, \quad (58)$$

and

$$\tilde{\mathbf{k}}_k = \frac{2\alpha_k^{(1)}}{N_0} \text{diag} \left\{ c, \alpha_k^{(2)}, c, \dots, \alpha_k^{(L_k)}, c \right\} \mathbf{t}_k, \quad (59)$$

where $\Upsilon_k \in \mathbb{R}^{(2\tilde{L}_k-1) \times (2\tilde{L}_k-1)}$ and $\mathbf{t}_k \in \mathbb{R}^{2\tilde{L}_k-1}$ are given by the matrix partition in (60) shown at the bottom of the page. Substituting (58) and (59) into (57), we obtain

$$\chi_k = \frac{1}{4\pi^2\beta^2} \mathbf{t}_k^T \Upsilon_k^{-1} \mathbf{t}_k, \quad (61)$$

which is independent of all the amplitudes.

Note that $0 \leq \chi_k \leq 1$: χ_k is nonnegative since it is a quadratic form and Υ_k is a positive semi-definite FIM (hence is Υ_k^{-1}); and $\chi_k \leq 1$ since the contribution from each anchor to the EFIM in (55) is nonnegative. \square

B. Proof of Corollary 1

Proof: This scenario can be thought of as a special case of Theorem 1 with $\tilde{L}_k = 1$, i.e., the first contiguous-cluster contains only one path. In this case, (61) becomes

$$\chi_k = \frac{1}{4\pi^2\beta^2} \frac{\dot{R}_s^2(1, 1)}{R_s(1, 1)}.$$

Since waveform $s(t)$ is continuous and time-limited in realistic cases, we have

$$\dot{R}_s(1, 1) = \left. \frac{\partial}{\partial \tau} R_s(\tau) \right|_{\tau=0} = 0,$$

implying that $\chi_k = 0$, which leads to (19). \square

$$\begin{bmatrix} \ddot{R}_s(1, 1) & \dot{R}_s(1, 1) \\ \dot{R}_s(1, 1) & R_s(1, 1) \\ \ddot{R}_s(1, 2) & -\dot{R}_s(1, 2) \\ \dot{R}_s(1, 2) & R_s(1, 2) \\ \vdots & \vdots \\ \dot{R}_s(1, \tilde{L}_k) & -\dot{R}_s(1, \tilde{L}_k) \\ \dot{R}_s(1, \tilde{L}_k) & R_s(1, \tilde{L}_k) \end{bmatrix} \triangleq \begin{bmatrix} \ddot{R}_s(1, 1) & \dot{R}_s(1, 1) & \ddot{R}_s(1, 2) & \dot{R}_s(1, 2) & \cdots & \ddot{R}_s(1, \tilde{L}_k) & \dot{R}_s(1, \tilde{L}_k) \\ \dot{R}_s(1, 1) & R_s(1, 1) & -\dot{R}_s(1, 2) & R_s(1, 2) & \cdots & -\dot{R}_s(1, \tilde{L}_k) & R_s(1, \tilde{L}_k) \\ \ddot{R}_s(1, 2) & -\dot{R}_s(1, 2) & & & & & \\ \dot{R}_s(1, 2) & R_s(1, 2) & & & & & \\ \vdots & \vdots & & & & & \\ \dot{R}_s(1, \tilde{L}_k) & -\dot{R}_s(1, \tilde{L}_k) & \cdots & & & \ddot{R}_s(\tilde{L}_k, \tilde{L}_k) & \dot{R}_s(\tilde{L}_k, \tilde{L}_k) \\ \dot{R}_s(1, \tilde{L}_k) & R_s(1, \tilde{L}_k) & \cdots & & & \dot{R}_s(\tilde{L}_k, \tilde{L}_k) & R_s(\tilde{L}_k, \tilde{L}_k) \end{bmatrix} \quad (60)$$

C. Proof of Theorem 2

Proof: When a priori channel knowledge of the channel is available, the FIM is

$$\mathbf{J}_\theta = \frac{1}{c^2} \begin{bmatrix} \mathbf{T}_{\text{NL}} \bar{\mathbf{\Lambda}}_{\text{NL}} \mathbf{T}_{\text{NL}}^T + \mathbf{T}_{\text{L}} \bar{\mathbf{\Lambda}}_{\text{L}} \mathbf{T}_{\text{L}}^T & \mathbf{T}_{\text{NL}} \bar{\mathbf{\Lambda}}_{\text{NL}} \\ \bar{\mathbf{\Lambda}}_{\text{NL}} \mathbf{T}_{\text{NL}}^T & \bar{\mathbf{\Lambda}}_{\text{NL}} \end{bmatrix} + \mathbf{J}_{\text{p}},$$

where $\bar{\mathbf{\Lambda}}_{\text{NL}} = \mathbb{E}_\theta \{ \mathbf{\Lambda}_{\text{NL}} \} \triangleq \text{diag} \{ \bar{\Psi}_1, \bar{\Psi}_2, \dots, \bar{\Psi}_M \}$ and $\bar{\mathbf{\Lambda}}_{\text{L}} = \mathbb{E}_\theta \{ \mathbf{\Lambda}_{\text{L}} \} \triangleq \text{diag} \{ \bar{\Psi}_{M+1}, \bar{\Psi}_{M+2}, \dots, \bar{\Psi}_{N_b} \}$. The FIM \mathbf{J}_θ can be partitioned as (12), where \mathbf{A} is given by (62) shown at the bottom of the page, and

$$\mathbf{B} \triangleq \begin{bmatrix} \mathbf{G}_{M+1} \bar{\Psi}_{M+1} + c^2 \bar{\Xi}_{\text{p},\kappa}^{M+1} & \dots & \mathbf{G}_{N_b} \bar{\Psi}_{N_b} + c^2 \bar{\Xi}_{\text{p},\kappa}^{N_b} \\ \mathbf{0} & \dots & \mathbf{0} \end{bmatrix},$$

and

$$\mathbf{C} \triangleq \text{diag} \left\{ \bar{\Psi}_{M+1} + c^2 \bar{\Xi}_{\kappa,\kappa}^{M+1}, \dots, \bar{\Psi}_{N_b} + c^2 \bar{\Xi}_{\kappa,\kappa}^{N_b} \right\}.$$

Apply the notion of EFI, and we have the 2×2 EFIM, after some algebra, given by (63) at the bottom of the page. From (9), we can rewrite $\bar{\Xi}_{\text{p},\text{p}}^k$ and $\bar{\Xi}_{\text{p},\kappa}^k$ in (11) using chain rule as

$$\bar{\Xi}_{\text{p},\text{p}}^k = \mathbf{q}_k \bar{\Xi}_{d,d}^k \mathbf{q}_k^T \quad \text{and} \quad \bar{\Xi}_{\text{p},\kappa}^k = \mathbf{q}_k \bar{\Xi}_{d,\kappa}^k, \quad (64)$$

where $\bar{\Xi}_{d,d}^k = \mathbf{F}_\theta(\boldsymbol{\kappa}_k | d_k; d_k, d_k)$ and $\bar{\Xi}_{d,\kappa}^k = \mathbf{F}_\theta(\boldsymbol{\kappa}_k | d_k; d_k, \boldsymbol{\kappa}_k)$. Substituting (64) into (63) leads to (21), where λ_k is given by (65a) and (65b) for LOS signals and NLOS signals, respectively, shown at the bottom of the page. \square

D. Proof of Corollary 2

Proof: We first show that the a priori channel knowledge increases the RII. Consider λ_k in (65a). Let

$$\mathbf{F}_k \triangleq \frac{1}{c^2} \begin{bmatrix} \mathbf{I}_k^T \bar{\Psi}_k \mathbf{I}_k + c^2 \bar{\Xi}_{d,d}^k & \mathbf{I}_k^T \bar{\Psi}_k \mathbf{D}_k^T + c^2 \bar{\Xi}_{d,\kappa}^k \\ \mathbf{D}_k \bar{\Psi}_k \mathbf{I}_k + c^2 \bar{\Xi}_{\text{p},\kappa}^{kT} & \mathbf{D}_k \bar{\Psi}_k \mathbf{D}_k^T + c^2 \bar{\Xi}_{\kappa,\kappa}^k \end{bmatrix},$$

and

$$\mathbf{E}_k \triangleq \frac{1}{c^2} \begin{bmatrix} \mathbf{I}_k^T \bar{\Psi}_k \mathbf{I}_k & \mathbf{I}_k^T \bar{\Psi}_k \mathbf{D}_k^T \\ \mathbf{D}_k \bar{\Psi}_k \mathbf{I}_k & \mathbf{D}_k \bar{\Psi}_k \mathbf{D}_k^T \end{bmatrix}.$$

We have $\mathbf{F}_k \succeq \mathbf{E}_k$, since

$$\mathbf{F}_k - \mathbf{E}_k = \begin{bmatrix} \bar{\Xi}_{d,d}^k & \bar{\Xi}_{d,\kappa}^k \\ \bar{\Xi}_{\text{p},\kappa}^{kT} & \bar{\Xi}_{\kappa,\kappa}^k \end{bmatrix} = \mathbf{F}_\theta(\boldsymbol{\kappa}_k | d_k; \tilde{\boldsymbol{\theta}}_k, \tilde{\boldsymbol{\theta}}_k) \succeq \mathbf{0},$$

where $\tilde{\boldsymbol{\theta}}_k = [d_k \ \boldsymbol{\kappa}_k^T]^T$. Hence we have $\lambda_k = 1/[\mathbf{F}_k^{-1}]_{1,1} \geq 1/[\mathbf{E}_k^{-1}]_{1,1}$, where $[\mathbf{E}_k^{-1}]_{1,1}$ equals (16). This implies that the a priori channel knowledge can increase the RII.

We next show that the RIIs in (65a) and (65b) reduce to (16) and zero, respectively, in the absence of a priori channel knowledge.

When a priori channel knowledge is unavailable, $\bar{\Xi}_{\kappa,\kappa}^k$, $\bar{\Xi}_{\text{p},\kappa}^k$, and $\bar{\Xi}_{\text{p},\text{p}}^k$ all equal zero, and the corresponding RII λ_k in (65a) and (65b) becomes

$$\begin{aligned} \lambda_k &= \frac{1}{c^2} \left\{ \mathbf{I}_k^T \bar{\Psi}_k \mathbf{I}_k - (\mathbf{I}_k^T \bar{\Psi}_k \mathbf{D}_k^T) (\mathbf{D}_k \bar{\Psi}_k \mathbf{D}_k^T)^{-1} (\mathbf{D}_k \bar{\Psi}_k \mathbf{I}_k) \right\} \\ &= \frac{1}{c^2} \mathbf{I}_k^T \left\{ \begin{bmatrix} 8\pi^2 \beta^2 \text{SNR}_k^{(1)} & \mathbf{k}_k^T \\ \mathbf{k}_k & \check{\Psi}_k \end{bmatrix} \right. \\ &\quad \left. - \begin{bmatrix} \mathbf{k}_k^T \\ \check{\Psi}_k \end{bmatrix} \check{\Psi}_k^{-1} \begin{bmatrix} \mathbf{k}_k & \check{\Psi}_k \end{bmatrix} \right\} \mathbf{I}_k \\ &= \frac{1}{c^2} \left\{ 8\pi^2 \beta^2 \text{SNR}_k^{(1)} - \mathbf{k}_k^T \check{\Psi}_k^{-1} \mathbf{k}_k \right\} \\ &= \frac{8\pi^2 \beta^2}{c^2} (1 - \chi_k) \text{SNR}_k^{(1)}, \end{aligned}$$

for $k \in \mathcal{N}_{\text{L}}$, and

$$\lambda_k = \frac{1}{c^2} \left\{ \mathbf{I}_k^T \bar{\Psi}_k \mathbf{I}_k - \mathbf{I}_k^T \bar{\Psi}_k \bar{\Psi}_k^{-1} \bar{\Psi}_k \mathbf{I}_k \right\} = 0,$$

for $k \in \mathcal{N}_{\text{NL}}$. \square

$$\mathbf{A} \triangleq \begin{bmatrix} \sum_{k \in \mathcal{N}_b} \mathbf{G}_k \bar{\Psi}_k \mathbf{G}_k^T + c^2 \bar{\Xi}_{\text{p},\text{p}}^k & \mathbf{G}_1 \bar{\Psi}_1 \mathbf{D}_1^T + c^2 \bar{\Xi}_{\text{p},\kappa}^1 & \dots & \mathbf{G}_M \bar{\Psi}_M \mathbf{D}_M^T + c^2 \bar{\Xi}_{\text{p},\kappa}^M \\ (\mathbf{G}_1 \bar{\Psi}_1 \mathbf{D}_1^T + c^2 \bar{\Xi}_{\text{p},\kappa}^1)^T & \mathbf{D}_1 \bar{\Psi}_1 \mathbf{D}_1^T + c^2 \bar{\Xi}_{\kappa,\kappa}^1 & & \\ \vdots & & \ddots & \\ (\mathbf{G}_M \bar{\Psi}_M \mathbf{D}_M^T + c^2 \bar{\Xi}_{\text{p},\kappa}^M)^T & & & \mathbf{D}_M \bar{\Psi}_M \mathbf{D}_M^T + c^2 \bar{\Xi}_{\kappa,\kappa}^M \end{bmatrix} \quad (62)$$

$$\begin{aligned} \mathbf{J}_e(\mathbf{p}) &= \frac{1}{c^2} \left\{ \sum_{k \in \mathcal{N}_b} (\mathbf{G}_k \bar{\Psi}_k \mathbf{G}_k^T + c^2 \bar{\Xi}_{\text{p},\text{p}}^k) - \sum_{k \in \mathcal{N}_{\text{L}}} (\mathbf{G}_k \bar{\Psi}_k \mathbf{D}_k^T + c^2 \bar{\Xi}_{\text{p},\kappa}^k) (\mathbf{D}_k \bar{\Psi}_k \mathbf{D}_k^T + c^2 \bar{\Xi}_{\kappa,\kappa}^k)^{-1} (\mathbf{G}_k \bar{\Psi}_k \mathbf{D}_k^T + c^2 \bar{\Xi}_{\text{p},\kappa}^k)^T \right. \\ &\quad \left. - \sum_{k \in \mathcal{N}_{\text{NL}}} (\mathbf{G}_k \bar{\Psi}_k + c^2 \bar{\Xi}_{\text{p},\kappa}^k) (\bar{\Psi}_k + c^2 \bar{\Xi}_{\kappa,\kappa}^k)^{-1} (\mathbf{G}_k \bar{\Psi}_k + c^2 \bar{\Xi}_{\text{p},\kappa}^k)^T \right\} \quad (63) \end{aligned}$$

$$\lambda_k \triangleq \begin{cases} \frac{1}{c^2} \left\{ \mathbf{I}_k^T \bar{\Psi}_k \mathbf{I}_k + c^2 \bar{\Xi}_{d,d}^k - (\mathbf{I}_k^T \bar{\Psi}_k \mathbf{D}_k^T + c^2 \bar{\Xi}_{d,\kappa}^k) (\mathbf{D}_k \bar{\Psi}_k \mathbf{D}_k^T + c^2 \bar{\Xi}_{\kappa,\kappa}^k)^{-1} (\mathbf{I}_k^T \bar{\Psi}_k \mathbf{D}_k^T + c^2 \bar{\Xi}_{d,\kappa}^k)^T \right\}, & k \in \mathcal{N}_{\text{L}} \quad (65a) \\ \frac{1}{c^2} \left\{ \mathbf{I}_k^T \bar{\Psi}_k \mathbf{I}_k + c^2 \bar{\Xi}_{d,d}^k - (\mathbf{I}_k^T \bar{\Psi}_k + c^2 \bar{\Xi}_{d,\kappa}^k) (\bar{\Psi}_k + c^2 \bar{\Xi}_{\kappa,\kappa}^k)^{-1} (\mathbf{I}_k^T \bar{\Psi}_k + c^2 \bar{\Xi}_{d,\kappa}^k)^T \right\}, & k \in \mathcal{N}_{\text{NL}} \quad (65b) \end{cases}$$

E. Proof of Corollary 3

Proof: The block matrices $\Xi_{\kappa,\kappa}^k$ and $\Xi_{d,\kappa}^k$ in (11) for NLOS signals can be written as

$$\Xi_{\kappa,\kappa}^k = \begin{bmatrix} t^2 & \mathbf{v}_k^T \\ \mathbf{v}_k & \check{\Xi}_{\kappa,\kappa}^k \end{bmatrix} \quad \text{and} \quad \Xi_{d,\kappa}^k = \begin{bmatrix} w & \check{\Xi}_{d,\kappa}^k \end{bmatrix},$$

where $\mathbf{v}_k, \check{\Xi}_{d,\kappa}^k \in \mathbb{R}^{2L_k-1}$, and $\check{\Xi}_{\kappa,\kappa}^k \in \mathbb{R}^{(2L_k-1) \times (2L_k-1)}$. Note that t^2 corresponds to the Fisher information of $b_k^{(1)}$. When the a priori knowledge of $b_k^{(1)}$ goes to ∞ , i.e., $g_b(b_k^{(1)}) \rightarrow \delta(b_k^{(1)})$, we claim that

$$\begin{aligned} & \lim_{t^2 \rightarrow \infty} \left[\bar{\Psi}_k + c^2 \Xi_{\kappa,\kappa}^k \right]^{-1} \\ &= \begin{bmatrix} 0 & \mathbf{0}^T \\ \mathbf{0} & \left(\mathbf{D}_k \bar{\Psi}_k \mathbf{D}_k^T + c^2 \check{\Xi}_{\kappa,\kappa}^k \right)^{-1} \end{bmatrix}. \end{aligned} \quad (66)$$

To show this, we partition $\bar{\Psi}_k$ as

$$\bar{\Psi}_k = \begin{bmatrix} u_k^2 & \mathbf{k}_k^T \\ \mathbf{k}_k & \check{\Psi}_k \end{bmatrix},$$

and then the left-hand-side of (66) becomes

$$\begin{aligned} \text{LHS} &= \lim_{t^2 \rightarrow \infty} \begin{bmatrix} u_k^2 + c^2 t^2 & \mathbf{k}_k^T + c^2 \mathbf{v}_k^T \\ \mathbf{k}_k + c^2 \mathbf{v}_k & \check{\Psi}'_k + c^2 \check{\Xi}_{\kappa,\kappa}^k \end{bmatrix}^{-1} \\ &= \lim_{t^2 \rightarrow \infty} \begin{bmatrix} A & B \\ B^T & C \end{bmatrix}, \end{aligned}$$

where

$$A \triangleq \begin{bmatrix} u_k^2 + c^2 t^2 \\ -(\mathbf{k}_k + c^2 \mathbf{v}_k)^T \left(\check{\Psi}_k + c^2 \check{\Xi}_{\kappa,\kappa}^k \right)^{-1} (\mathbf{k}_k + c^2 \mathbf{v}_k) \end{bmatrix}^{-1},$$

$$B \triangleq -\frac{1}{u_k^2 + c^2 t^2} (\mathbf{k}_k + c^2 \mathbf{v}_k) \mathbf{C}^{-1},$$

and

$$C \triangleq \begin{bmatrix} \check{\Psi}_k + c^2 \check{\Xi}_{\kappa,\kappa}^k \\ -\frac{1}{u_k^2 + c^2 t^2} (\mathbf{k}_k + c^2 \mathbf{v}_k) (\mathbf{k}_k + c^2 \mathbf{v}_k)^T \end{bmatrix}^{-1}.$$

When $b_k^{(1)}$ is known, i.e., $t^2 \rightarrow \infty$, we have $\lim_{t^2 \rightarrow \infty} A = 0$, $\lim_{t^2 \rightarrow \infty} B = \mathbf{0}$, and $\lim_{t^2 \rightarrow \infty} C = \left[\check{\Psi}_k + c^2 \check{\Xi}_{\kappa,\kappa}^k \right]^{-1}$.

Notice that $\check{\Psi}_k = \mathbf{D}_k \bar{\Psi}_k \mathbf{D}_k^T$. Hence, we proved our claim in (66).

Substituting (66) into (65b), we have

$$\begin{aligned} \lim_{t^2 \rightarrow \infty} \lambda_k &= \frac{1}{c^2} \left\{ \mathbf{1}_k^T \bar{\Psi}_k \mathbf{1}_k + c^2 \Xi_{d,d}^k - \left(\mathbf{1}_k^T \bar{\Psi}_k \mathbf{D}_k^T + c^2 \check{\Xi}_{d,\kappa}^k \right) \right. \\ &\quad \left. \times \left(\mathbf{D}_k \bar{\Psi}_k \mathbf{D}_k^T + c^2 \check{\Xi}_{\kappa,\kappa}^k \right)^{-1} \left(\mathbf{1}_k^T \bar{\Psi}_k \mathbf{D}_k^T + c^2 \check{\Xi}_{d,\kappa}^k \right)^T \right\}, \end{aligned}$$

for $k \in \mathcal{N}_{\text{NL}}$, which agrees with the RII of LOS signals in (65a).²⁹ Hence LOS signals are equivalent to NLOS with infinite a priori knowledge of $b_k^{(1)}$ for localization. \square

F. Proof of Proposition 2

Proof: Note that $\mathbf{q}_k, \bar{\Psi}_k, \Xi_{\mathbf{p},\mathbf{p}}^k, \Xi_{\kappa,\kappa}^k$, and $\Xi_{\mathbf{p},\kappa}^k$ are functions of \mathbf{p} when a priori knowledge of the agent's position is available. Hence we need to take expectation of them over \mathbf{p} in (10). After some algebra, we have the EFIM for the agent's position as (67) shown at the bottom of the page.

When the condition in (22) is satisfied for the functions $g(\mathbf{p})$'s: 1) $\mathbf{q}_k \Xi_{d,d}^k \mathbf{q}_k^T$, 2) $\mathbf{q}_k \mathbf{1}_k^T \bar{\Psi}_k \mathbf{1}_k \mathbf{q}_k^T$, 3) $\mathbf{q}_k \left(\mathbf{1}_k^T \bar{\Psi}_k + c^2 \Xi_{d,\kappa}^k \right)$, and 4) $\bar{\Psi}_k + \Xi_{\kappa,\kappa}^k$, we can approximate the expectation of each function over \mathbf{p} in (67) by the function value at the expected position $\bar{\mathbf{p}}$. Hence the EFIM in (67) can be expressed as

$$\begin{aligned} \mathbf{J}_e(\mathbf{p}) &= \Xi_{\mathbf{p}} + \frac{1}{c^2} \sum_{k \in \mathcal{N}_b} \left\{ \mathbf{q}_k \left(\mathbf{1}_k^T \bar{\Psi}_k \mathbf{1}_k + c^2 \Xi_{d,d}^k \right) \mathbf{q}_k^T \right. \\ &\quad \left. - \mathbf{q}_k \left(\mathbf{1}_k^T \bar{\Psi}_k + c^2 \Xi_{d,\kappa}^k \right) \left(\bar{\Psi}_k + \Xi_{\kappa,\kappa}^k \right)^{-1} \right. \\ &\quad \left. \times \left(\mathbf{1}_k^T \bar{\Psi}_k + c^2 \Xi_{d,\kappa}^k \right)^T \mathbf{q}_k^T \right\} \\ &= \Xi_{\mathbf{p}} + \sum_{k \in \mathcal{N}_b} \bar{\lambda}_k \mathbf{J}_r(\bar{\phi}_k), \end{aligned}$$

where $\bar{\phi}_k$ is the angle from anchor k to $\bar{\mathbf{p}}$, and $\bar{\lambda}_k$ is given by (68) shown at the bottom of the page. Note that all functions are evaluated at $\bar{\mathbf{p}}$. \square

²⁹Note that the size of $\Xi_{\kappa,\kappa}^k$ and $\Xi_{d,\kappa}^k$ for LOS signals and NLOS signals are different for the same L_k . Indeed, $\check{\Xi}_{\kappa,\kappa}^k$ and $\check{\Xi}_{d,\kappa}^k$ are not associated with $b_k^{(1)}$, and hence they are in the same form as $\Xi_{\kappa,\kappa}^k$ and $\Xi_{d,\kappa}^k$ for LOS signals in (65a).

$$\begin{aligned} \mathbf{J}_e(\mathbf{p}) &= \Xi_{\mathbf{p}} + \sum_{k \in \mathcal{N}_b} \left\{ \mathbb{E}_{\mathbf{p}} \left\{ \mathbf{q}_k \Xi_{d,d}^k \mathbf{q}_k^T \right\} + \frac{1}{c^2} \mathbb{E}_{\mathbf{p}} \left\{ \mathbf{q}_k \mathbf{1}_k^T \bar{\Psi}_k \mathbf{1}_k \mathbf{q}_k^T \right\} \right. \\ &\quad \left. - \frac{1}{c^2} \mathbb{E}_{\mathbf{p}} \left\{ \mathbf{q}_k \left(\mathbf{1}_k^T \bar{\Psi}_k + c^2 \Xi_{d,\kappa}^k \right) \right\} \mathbb{E}_{\mathbf{p}} \left\{ \bar{\Psi}_k + \Xi_{\kappa,\kappa}^k \right\}^{-1} \mathbb{E}_{\mathbf{p}} \left\{ \left(\mathbf{1}_k^T \bar{\Psi}_k + c^2 \Xi_{d,\kappa}^k \right)^T \mathbf{q}_k^T \right\} \right\} \end{aligned} \quad (67)$$

$$\bar{\lambda}_k \triangleq \frac{1}{c^2} \left\{ \mathbf{1}_k^T \bar{\Psi}_k \mathbf{1}_k + c^2 \Xi_{d,d}^k - \left(\mathbf{1}_k^T \bar{\Psi}_k + c^2 \Xi_{d,\kappa}^k \right) \left(\bar{\Psi}_k + c^2 \Xi_{\kappa,\kappa}^k \right)^{-1} \left(\mathbf{1}_k^T \bar{\Psi}_k + c^2 \Xi_{d,\kappa}^k \right)^T \right\} \quad (68)$$

APPENDIX D
PROOFS OF THE RESULTS IN SECTION IV

A. Proof of Theorem 3

Note that this proof also incorporates the a priori channel knowledge. In the absence of this knowledge, the corresponding results can be obtained by removing \mathbf{J}_p that characterizes the a priori channel knowledge.

Since \mathbf{p} and φ are deterministic but unknown, the joint likelihood function of the random vectors \mathbf{r} and $\boldsymbol{\theta}$ can be written as

$$f(\mathbf{r}, \boldsymbol{\theta}) = f(\mathbf{r}|\boldsymbol{\theta}) f(\boldsymbol{\theta}) = \prod_{n \in \mathcal{N}_a} \prod_{k \in \mathcal{N}_b} f(\mathbf{r}_{nk}|\boldsymbol{\theta}) f(\boldsymbol{\kappa}_{nk}|\mathbf{p}, \varphi).$$

Note that $f(\boldsymbol{\kappa}_{nk}|\mathbf{p}, \varphi) = f(\boldsymbol{\kappa}_{nk}|d_{nk})$, and the FIM \mathbf{J}_p from $f(\boldsymbol{\theta})$ can be expressed as (69) shown at the bottom of the page, where $\Xi_{\mathbf{p},\mathbf{p}}^{nk} = \mathbf{q}_{nk} \Xi_{d,\kappa}^{nk} \mathbf{q}_{nk}^T$, $\Xi_{\mathbf{p},\varphi}^{nk} = \mathbf{q}_{nk} \Xi_{d,d}^{nk} h_{nk}$, and $\Xi_{\varphi,\varphi}^{nk} = h_{nk}^2 \Xi_{d,d}^{nk}$ in which

$$\Xi_{d,d}^{nk} \triangleq \mathbf{F}_\theta(\mathbf{r}_{nk}|\boldsymbol{\theta}; d_{nk}, d_{nk}).$$

Block matrices $\Xi_{\mathbf{p},n}$, $\Xi_{\varphi,n}$, and Ξ_n correspond to the n th antenna in the array, and they can be further decomposed into block matrices corresponding to each anchor:

$$\begin{aligned} \Xi_{\mathbf{p},n} &= \begin{bmatrix} \Xi_{\mathbf{p},\kappa}^{n,1} & \Xi_{\mathbf{p},\kappa}^{n,2} & \cdots & \Xi_{\mathbf{p},\kappa}^{n,N_b} \end{bmatrix}, \\ \Xi_{\varphi,n} &= \begin{bmatrix} \Xi_{\varphi,\kappa}^{n,1} & \Xi_{\varphi,\kappa}^{n,2} & \cdots & \Xi_{\varphi,\kappa}^{n,N_b} \end{bmatrix}, \end{aligned}$$

and

$$\Xi_n = \text{diag} \left\{ \Xi_{\kappa,\kappa}^{n,1}, \Xi_{\kappa,\kappa}^{n,2}, \dots, \Xi_{\kappa,\kappa}^{n,N_b} \right\},$$

where $\Xi_{\mathbf{p},\kappa}^{nk} = \mathbf{q}_{nk} \Xi_{d,\kappa}^{nk}$ and $\Xi_{\varphi,\kappa}^{nk} = h_{nk} \Xi_{d,\kappa}^{nk}$, and $\Xi_{\kappa,\kappa}^{nk} = \mathbf{F}_\theta(\boldsymbol{\kappa}_{nk}|\mathbf{p}, \varphi; \boldsymbol{\kappa}_{nk}, \boldsymbol{\kappa}_{nk})$, in which $\Xi_{d,\kappa}^{nk} = \mathbf{F}_\theta(\boldsymbol{\kappa}_{nk}|\mathbf{p}, \varphi; d_{nk}, \boldsymbol{\kappa}_{nk})$.

Similar to the proof of Theorem 2 in Appendix C-C, the FIM from observation can be obtained as (70) shown at the bottom of the page, where

$$\begin{aligned} \mathbf{G}_n &= \begin{bmatrix} \mathbf{q}_{n,1} \mathbf{1}_{n,1}^T & \mathbf{q}_{n,2} \mathbf{1}_{n,2}^T & \cdots & \mathbf{q}_{n,N_b} \mathbf{1}_{n,N_b}^T \end{bmatrix}, \\ \mathbf{h}_n &= \begin{bmatrix} h_{n,1} \mathbf{1}_{n,1}^T & h_{n,2} \mathbf{1}_{n,2}^T & \cdots & h_{n,N_b} \mathbf{1}_{n,N_b}^T \end{bmatrix}, \end{aligned}$$

and

$$\bar{\Lambda}_n = \text{diag} \{ \bar{\Psi}_{n,1}, \bar{\Psi}_{n,2}, \dots, \bar{\Psi}_{n,N_b} \}$$

correspond to the n th antenna as defined in (44).

The overall FIM \mathbf{J}_θ is the sum of (69) and (70). By applying the notion of EFI, we have the 3×3 EFIM for the position and the orientation as follows

$$\mathbf{J}_e(\mathbf{p}, \varphi) = \sum_{n \in \mathcal{N}_a} \sum_{k \in \mathcal{N}_b} \begin{bmatrix} \lambda_{nk} \mathbf{q}_{nk} \mathbf{q}_{nk}^T & \lambda_{nk} h_{nk} \mathbf{q}_{nk} \\ \lambda_{nk} h_{nk} \mathbf{q}_{nk}^T & \lambda_{nk} h_{nk}^2 \end{bmatrix}, \quad (71)$$

where λ_{nk} is given by (72) shown at the bottom of the page.

Note that in the absence of a priori channel knowledge, the above result is still valid, with the RII of (72) degenerating to (73) shown at the bottom of the page, where $\mathbf{D}_{nk} = \begin{bmatrix} \mathbf{0} & \mathbf{I}_{2L_{nk}-1} \end{bmatrix}$.

B. Proof of Proposition 3

Since $\mathbf{q}\mathbf{q}^T$ is always positive semi-definite, we need to simply prove that there exists a unique \mathbf{p}^* such that $\mathbf{q}^* = \mathbf{0}$.

$$\mathbf{J}_p = \begin{bmatrix} \sum_{n \in \mathcal{N}_a} \sum_{k \in \mathcal{N}_b} \Xi_{\mathbf{p},\mathbf{p}}^{nk} & \sum_{n \in \mathcal{N}_a} \sum_{k \in \mathcal{N}_b} \Xi_{\mathbf{p},\varphi}^{nk} & \Xi_{\mathbf{p},1} & \cdots & \Xi_{\mathbf{p},N_a} \\ \sum_{n \in \mathcal{N}_a} \sum_{k \in \mathcal{N}_b} \Xi_{\mathbf{p},\varphi}^{nk T} & \sum_{n \in \mathcal{N}_a} \sum_{k \in \mathcal{N}_b} \Xi_{\varphi,\varphi}^{nk} & \Xi_{\varphi,1} & \cdots & \Xi_{\varphi,N_a} \\ \Xi_{\mathbf{p},1}^T & \Xi_{\varphi,1}^T & \Xi_1 & & \\ \vdots & \vdots & & \ddots & \\ \Xi_{\mathbf{p},N_a}^T & \Xi_{\varphi,N_a}^T & & & \Xi_{N_a} \end{bmatrix} \quad (69)$$

$$\mathbf{J}_w = \frac{1}{c^2} \begin{bmatrix} \sum_{n \in \mathcal{N}_a} \mathbf{G}_n \bar{\Lambda}_n \mathbf{G}_n^T & \sum_{n \in \mathcal{N}_a} \mathbf{G}_n \bar{\Lambda}_n \mathbf{h}_n^T & \mathbf{G}_1 \bar{\Lambda}_1 & \cdots & \mathbf{G}_{N_a} \bar{\Lambda}_{N_a} \\ \sum_{n \in \mathcal{N}_a} \mathbf{h}_n \bar{\Lambda}_n \mathbf{G}_n^T & \sum_{n \in \mathcal{N}_a} \mathbf{h}_n \bar{\Lambda}_n \mathbf{h}_n^T & \mathbf{h}_1 \bar{\Lambda}_1 & \cdots & \mathbf{h}_{N_a} \bar{\Lambda}_{N_a} \\ \bar{\Lambda}_1 \mathbf{G}_1^T & \bar{\Lambda}_1 \mathbf{h}_1^T & \bar{\Lambda}_1 & & \\ \vdots & \vdots & & \ddots & \\ \bar{\Lambda}_{N_a} \mathbf{G}_{N_a}^T & \bar{\Lambda}_{N_a} \mathbf{h}_{N_a}^T & & & \bar{\Lambda}_{N_a} \end{bmatrix} \quad (70)$$

$$\lambda_{nk} \triangleq \frac{1}{c^2} \left\{ \mathbf{1}_{nk}^T \bar{\Psi}_{nk} \mathbf{1}_{nk} + c^2 \Xi_{d,d}^{nk} - \left(\mathbf{1}_{nk}^T \bar{\Psi}_{nk} + c^2 \Xi_{d,\kappa}^{nk} \right) \left(\bar{\Psi}_{nk} + c^2 \Xi_{\kappa,\kappa}^{nk} \right)^{-1} \left(\mathbf{1}_{nk}^T \bar{\Psi}_{nk} + c^2 \Xi_{d,\kappa}^{nk} \right)^T \right\} \quad (72)$$

$$\lambda_{nk} = \begin{cases} \mathbf{1}_{nk}^T \left\{ \bar{\Psi}_{nk} - (\bar{\Psi}_{nk} \mathbf{D}_{nk}^T) (\mathbf{D}_{nk} \bar{\Psi}_{nk} \mathbf{D}_{nk}^T)^{-1} (\mathbf{D}_{nk} \bar{\Psi}_{nk}) \right\} \mathbf{1}_{nk} / c^2, & \text{LOS} \\ 0, & \text{NLOS} \end{cases} \quad (73)$$

Proof: Let \mathbf{p} be an arbitrary reference point, and

$$\mathbf{p}^* = \mathbf{p} + \mathbf{g}(\varphi),$$

where $\mathbf{g}(\varphi) = [g_x(\varphi) \ g_y(\varphi)]^T$, and $g_x(\varphi)$ and $g_y(\varphi)$ denote the relative distance in x and y directions, respectively. Then, h_{nk} corresponding to \mathbf{p} can be written as a sum of two parts

$$h_{nk} = h_{nk}^* + \tilde{h}_{nk},$$

where h_{nk}^* corresponds to \mathbf{p}^*

$$h_{nk}^* = \frac{d}{d\varphi} \Delta x_n(\mathbf{p}^*, \varphi) \cos \phi_{nk} + \frac{d}{d\varphi} \Delta y_n(\mathbf{p}^*, \varphi) \sin \phi_{nk},$$

and

$$\begin{aligned} \tilde{h}_{nk} &= \frac{d}{d\varphi} g_x(\varphi) \cos \phi_{nk} + \frac{d}{d\varphi} g_y(\varphi) \sin \phi_{nk} \\ &\triangleq \dot{g}_x \cos \phi_{nk} + \dot{g}_y \sin \phi_{nk} = \dot{\mathbf{g}}^T \mathbf{q}_{nk}. \end{aligned}$$

Hence, \mathbf{q} corresponding to the reference position \mathbf{p} is given by

$$\mathbf{q} = \underbrace{\sum_{n \in \mathcal{N}_a} \sum_{k \in \mathcal{N}_b} \lambda_{nk} h_{nk}^* \mathbf{q}_{nk}}_{\triangleq \mathbf{q}^*} + \underbrace{\sum_{n \in \mathcal{N}_a} \sum_{k \in \mathcal{N}_b} \lambda_{nk} \tilde{h}_{nk} \mathbf{q}_{nk}}_{\triangleq \tilde{\mathbf{q}}}, \quad (74)$$

and $\tilde{\mathbf{q}}$ can be written as

$$\begin{aligned} \tilde{\mathbf{q}} &= \sum_{n \in \mathcal{N}_a} \sum_{k \in \mathcal{N}_b} \mathbf{q}_{nk}^T \dot{\mathbf{g}} \lambda_{nk} \mathbf{q}_{nk} \\ &= \sum_{n \in \mathcal{N}_a} \sum_{k \in \mathcal{N}_b} \lambda_{nk} \mathbf{q}_{nk} \mathbf{q}_{nk}^T \dot{\mathbf{g}} = \sum_{n \in \mathcal{N}_a} \mathbf{J}_{e,n} \dot{\mathbf{g}}. \end{aligned} \quad (75)$$

Since $\sum_{n \in \mathcal{N}_a} \mathbf{J}_{e,n} \succ \mathbf{0}$, we have $\mathbf{q}^* = \mathbf{0}$ if and only if

$$\dot{\mathbf{g}} = \left(\sum_{n \in \mathcal{N}_a} \mathbf{J}_{e,n} \right)^{-1} \mathbf{q},$$

implying that there exists only one $\dot{\mathbf{g}}$, and hence only one $\mathbf{g}(\varphi)$, such that $\mathbf{q}^* = \mathbf{0}$. Therefore, the orientation center \mathbf{p}^* is unique. \square

C. Proof of Corollary 5

Proof: We first prove that the SOEB is independent of the reference point \mathbf{p} . It is equivalent to show that the EFI for the orientation given by (27) equals the EFI for the orientation based on \mathbf{p}^* , given by

$$J_e^*(\varphi) = \sum_{n \in \mathcal{N}_a} \sum_{k \in \mathcal{N}_b} \lambda_{nk} h_{nk}^{*2}.$$

Let $\mathbf{J} = \sum_{n \in \mathcal{N}_a} \mathbf{J}_{e,n}$. From (74) and (75), we have $\mathbf{q} = \tilde{\mathbf{q}} + \mathbf{J} \dot{\mathbf{g}}$, and hence

$$\mathbf{q}^T \mathbf{J}^{-1} \mathbf{q} = \tilde{\mathbf{q}}^T \mathbf{J}^{-1} \tilde{\mathbf{q}} + \tilde{\mathbf{q}}^T \dot{\mathbf{g}} = \sum_{n \in \mathcal{N}_a} \sum_{k \in \mathcal{N}_b} \lambda_{nk} \tilde{h}_{nk}^2.$$

On the other hand, we also have

$$\sum_{n \in \mathcal{N}_a} \sum_{k \in \mathcal{N}_b} \lambda_{nk} h_{nk}^* \tilde{h}_{nk} = \mathbf{q}^* \dot{\mathbf{g}} = 0.$$

Therefore, we can verify that the EFI for the orientation in (27)

$$\begin{aligned} J_e(\varphi) &= \sum_{n \in \mathcal{N}_a} \sum_{k \in \mathcal{N}_b} \lambda_{nk} (h_{nk}^* + \tilde{h}_{nk})^2 - \tilde{\mathbf{q}}^T \mathbf{J}^{-1} \tilde{\mathbf{q}} \\ &= \sum_{n \in \mathcal{N}_a} \sum_{k \in \mathcal{N}_b} \lambda_{nk} h_{nk}^{*2} + 2 \sum_{n \in \mathcal{N}_a} \sum_{k \in \mathcal{N}_b} \lambda_{nk} h_{nk}^* \tilde{h}_{nk} \\ &= J_e^*(\varphi). \end{aligned} \quad (76)$$

This shows that the EFI for the orientation is independent of the reference point, and thus is the SOEB.

We next derive the SPEB for any reference point given in (32). The 3×3 EFIM in (71) can be written, using (74) and (76), as

$$\mathbf{J}_e(\mathbf{p}, \varphi) = \begin{bmatrix} \mathbf{J} & \tilde{\mathbf{q}} \\ \tilde{\mathbf{q}}^T & J_e(\varphi) + \tilde{\mathbf{q}}^T \mathbf{J}^{-1} \tilde{\mathbf{q}} \end{bmatrix}.$$

Using the equation of Shur's complement [66], we have

$$\begin{aligned} \mathbf{J}_e^{-1}(\mathbf{p}) &= \mathbf{J}^{-1} + \frac{1}{J_e(\varphi)} (\mathbf{J}^{-1} \tilde{\mathbf{q}}) (\mathbf{J}^{-1} \tilde{\mathbf{q}})^T \\ &= \mathbf{J}^{-1} + \frac{1}{J_e(\varphi)} \dot{\mathbf{g}} \dot{\mathbf{g}}^T. \end{aligned} \quad (77)$$

Since the translation $\mathbf{g}(\varphi)$ can be represented as

$$\mathbf{g}(\varphi) = \|\mathbf{p} - \mathbf{p}^*\| \begin{bmatrix} \cos(\varphi + \varphi_0) \\ \sin(\varphi + \varphi_0) \end{bmatrix},$$

where φ_0 is a constant angle, we have $\|\dot{\mathbf{g}}\| = \|\mathbf{p} - \mathbf{p}^*\|$. Then, by taking the trace of both sides of (77), we obtain

$$\begin{aligned} \mathcal{P}(\mathbf{p}) &= \mathcal{P}(\mathbf{p}^*) + \frac{\dot{\mathbf{g}}^T \dot{\mathbf{g}}}{J_e(\varphi)} \\ &= \mathcal{P}(\mathbf{p}^*) + \|\mathbf{p} - \mathbf{p}^*\|^2 \cdot \mathcal{P}(\varphi). \end{aligned}$$

\square

D. Proof of Proposition 5

Proof: Take the array center \mathbf{p}_0 as the reference point, and we have

$$\begin{aligned} \sum_{n \in \mathcal{N}_a} h_{nk} &= \sum_{n \in \mathcal{N}_a} \frac{d}{d\varphi} \Delta x_n(\mathbf{p}_0, \varphi) \cos \phi_{nk} \\ &\quad + \sum_{n \in \mathcal{N}_a} \frac{d}{d\varphi} \Delta y_n(\mathbf{p}_0, \varphi) \sin \phi_{nk} \\ &= \frac{d}{d\varphi} \left(\sum_{n \in \mathcal{N}_a} \Delta x_n(\mathbf{p}_0, \varphi) \right) \cos \phi_{nk} \\ &\quad + \frac{d}{d\varphi} \left(\sum_{n \in \mathcal{N}_a} \Delta y_n(\mathbf{p}_0, \varphi) \right) \sin \phi_{nk} \\ &= 0. \end{aligned}$$

Consequently,

$$\mathbf{q} = \sum_{n \in \mathcal{N}_a} \sum_{k \in \mathcal{N}_b} \lambda_k h_{nk} \mathbf{q}_k = \sum_{k \in \mathcal{N}_b} \left(\sum_{n \in \mathcal{N}_a} h_{nk} \right) \lambda_k \mathbf{q}_k = 0,$$

implying $\mathbf{p}_0 = \mathbf{p}^*$, i.e., the array center is the orientation center. \square

APPENDIX E
PROOFS OF THE RESULTS IN SECTION V

A. Proof of Theorem 4

In the presence of a time offset, the FIM can be written as (78) shown at the bottom of the page, where

$$\mathbf{J}_p = \begin{bmatrix} \sum_{k \in \mathcal{N}_b} \Xi_{p,p}^k & \mathbf{0} & \Xi_{p,\kappa}^1 & \cdots & \Xi_{p,\kappa}^{N_b} \\ \mathbf{0}^T & \Xi_B & \mathbf{0}^T & \cdots & \mathbf{0}^T \\ \Xi_{p,\kappa}^1{}^T & \mathbf{0} & \Xi_{\kappa,\kappa}^1 & & \\ \vdots & \vdots & & \ddots & \\ \Xi_{p,\kappa}^{N_b}{}^T & \mathbf{0} & & & \Xi_{\kappa,\kappa}^{N_b} \end{bmatrix}.$$

Applying the notion of EFI, we obtain the 3×3 EFIM

$$\mathbf{J}_e(\mathbf{p}, B) = \begin{bmatrix} \sum_{k \in \mathcal{N}_b} \lambda_k \mathbf{q}_k \mathbf{q}_k^T & \sum_{k \in \mathcal{N}_b} \lambda_k \mathbf{q}_k \\ \sum_{k \in \mathcal{N}_b} \lambda_k \mathbf{q}_k^T & \sum_{k \in \mathcal{N}_b} \lambda_k + \Xi_B \end{bmatrix},$$

where λ_k is given by (65b), and another step of EFI leads to (34) and (35).

B. Proof of Theorem 5

We consider orientation-unaware case, whereas orientation-aware case is a special case with a reduced parameter set. The FIM using an antenna array can be written as (79) shown at the bottom of the page, where $\mathbf{l}_n = [\mathbf{l}_{n,1}^T \ \mathbf{l}_{n,2}^T \ \cdots \ \mathbf{l}_{n,N_b}^T]^T$, and \mathbf{J}_p is given by (80) shown at the bottom of the page. Applying the notion of EFI to \mathbf{J}_θ , we obtain the 4×4 EFIM in (37).

C. Proof of Corollary 8

We incorporate the a priori knowledge of the array center and orientation into (37), and obtain the EFIM in far-field scenarios as (81) shown at the bottom of the page. Recall that in far-field scenarios, $\mathbf{p}_0 = \mathbf{p}^*$, implying that $\sum_{n \in \mathcal{N}_a} \sum_{k \in \mathcal{N}_b} \lambda_{nk} h_{nk} \mathbf{q}_{nk} = \mathbf{0}$ and $\sum_{n \in \mathcal{N}_a} \sum_{k \in \mathcal{N}_b} \lambda_{nk} h_{nk} = 0$. Also, we have $\bar{\lambda}_{nk} = \bar{\lambda}_k$ and $\bar{\phi}_{nk} = \bar{\phi}_k$ for all n , and hence the EFIM can be written as (82) shown at the top of the next page, where \bar{h}_{nk} and $\bar{\mathbf{q}}_k$ is a function of $\bar{\mathbf{p}}_0$.

$$\mathbf{J}_\theta = \frac{1}{c^2} \begin{bmatrix} \sum_{k \in \mathcal{N}_b} \mathbf{G}_k \bar{\Psi}_k \mathbf{G}_k^T & \sum_{k \in \mathcal{N}_b} \mathbf{G}_k \bar{\Psi}_k \mathbf{l}_k & \mathbf{G}_1 \bar{\Psi}_1 & \cdots & \mathbf{G}_{N_b} \bar{\Psi}_{N_b} \\ \sum_{k \in \mathcal{N}_b} \mathbf{l}_k^T \bar{\Psi}_k \mathbf{G}_k & \sum_{k \in \mathcal{N}_b} \mathbf{l}_k^T \bar{\Psi}_k \mathbf{l}_k & \mathbf{l}_1^T \bar{\Psi}_1 & \cdots & \mathbf{l}_{N_b}^T \bar{\Psi}_{N_b} \\ \bar{\Psi}_1 \mathbf{G}_1^T & \bar{\Psi}_1 \mathbf{l}_1 & \bar{\Psi}_1 & & \\ \vdots & \vdots & & \ddots & \\ \bar{\Psi}_{N_b} \mathbf{G}_{N_b}^T & \bar{\Psi}_{N_b} \mathbf{l}_{N_b} & & & \bar{\Psi}_{N_b} \end{bmatrix} + \mathbf{J}_p \quad (78)$$

$$\mathbf{J}_\theta = \frac{1}{c^2} \begin{bmatrix} \sum_{n \in \mathcal{N}_a} \mathbf{G}_n \bar{\Lambda}_n \mathbf{G}_n^T & \sum_{n \in \mathcal{N}_a} \mathbf{G}_n \bar{\Lambda}_n \mathbf{h}_n^T & \sum_{n \in \mathcal{N}_a} \mathbf{G}_n \bar{\Lambda}_n \mathbf{l}_n^T & \mathbf{G}_1 \bar{\Lambda}_1 & \cdots & \mathbf{G}_{N_a} \bar{\Lambda}_{N_a} \\ \sum_{n \in \mathcal{N}_a} \mathbf{h}_n \bar{\Lambda}_n \mathbf{G}_n^T & \sum_{n \in \mathcal{N}_a} \mathbf{h}_n \bar{\Lambda}_n \mathbf{h}_n^T & \sum_{n \in \mathcal{N}_a} \mathbf{h}_n \bar{\Lambda}_n \mathbf{l}_n^T & \mathbf{h}_1 \bar{\Lambda}_1 & \cdots & \mathbf{h}_{N_a} \bar{\Lambda}_{N_a} \\ \sum_{n \in \mathcal{N}_a} \mathbf{l}_n \bar{\Lambda}_n \mathbf{G}_n^T & \sum_{n \in \mathcal{N}_a} \mathbf{l}_n \bar{\Lambda}_n \mathbf{h}_n^T & \sum_{n \in \mathcal{N}_a} \mathbf{l}_n \bar{\Lambda}_n \mathbf{l}_n^T & \mathbf{l}_1 \bar{\Lambda}_1 & \cdots & \mathbf{l}_{N_a} \bar{\Lambda}_{N_a} \\ \bar{\Lambda}_1 \mathbf{G}_1^T & \bar{\Lambda}_1 \mathbf{h}_1^T & \bar{\Lambda}_1 \mathbf{l}_1^T & \bar{\Lambda}_1 & & \\ \vdots & \vdots & \vdots & & \ddots & \\ \bar{\Lambda}_{N_a} \mathbf{G}_{N_a}^T & \bar{\Lambda}_{N_a} \mathbf{h}_{N_a}^T & \bar{\Lambda}_{N_a} \mathbf{l}_{N_a}^T & & & \bar{\Lambda}_{N_a} \end{bmatrix} + \mathbf{J}_p \quad (79)$$

$$\mathbf{J}_p = \begin{bmatrix} \sum_{n \in \mathcal{N}_a} \sum_{k \in \mathcal{N}_b} \Xi_{p,p}^{nk} & \sum_{n \in \mathcal{N}_a} \sum_{k \in \mathcal{N}_b} \Xi_{p,\varphi}^{nk} & \mathbf{0} & \Xi_{p,1} & \cdots & \Xi_{p,N_a} \\ \sum_{n \in \mathcal{N}_a} \sum_{k \in \mathcal{N}_b} \Xi_{p,\varphi}^{nk}{}^T & \sum_{n \in \mathcal{N}_a} \sum_{k \in \mathcal{N}_b} \Xi_{\varphi,\varphi}^{nk} & \mathbf{0} & \Xi_{\varphi,1} & \cdots & \Xi_{\varphi,N_a} \\ \mathbf{0}^T & \mathbf{0} & \Xi_B & \mathbf{0}^T & \cdots & \mathbf{0}^T \\ \Xi_{p,1}^T & \Xi_{\varphi,1}^T & \mathbf{0} & \Xi_1 & & \\ \vdots & \vdots & \vdots & & \ddots & \\ \Xi_{p,N_a}^T & \Xi_{\varphi,N_a}^T & \mathbf{0} & & & \Xi_{N_a} \end{bmatrix} \quad (80)$$

$$\mathbf{J}_e^{\text{Array-B}} = \begin{bmatrix} \sum_{n \in \mathcal{N}_a} \sum_{k \in \mathcal{N}_b} \bar{\lambda}_{nk} \mathbf{q}_{nk} \mathbf{q}_{nk}^T + \Xi_p & \sum_{n \in \mathcal{N}_a} \sum_{k \in \mathcal{N}_b} \bar{\lambda}_{nk} h_{nk} \mathbf{q}_{nk} & \sum_{n \in \mathcal{N}_a} \sum_{k \in \mathcal{N}_b} \bar{\lambda}_{nk} \mathbf{q}_{nk} \\ \sum_{n \in \mathcal{N}_a} \sum_{k \in \mathcal{N}_b} \bar{\lambda}_{nk} h_{nk} \mathbf{q}_{nk}^T & \sum_{n \in \mathcal{N}_a} \sum_{k \in \mathcal{N}_b} \bar{\lambda}_{nk} h_{nk}^2 + \Xi_\varphi & \sum_{n \in \mathcal{N}_a} \sum_{k \in \mathcal{N}_b} \bar{\lambda}_{nk} h_{nk} \\ \sum_{n \in \mathcal{N}_a} \sum_{k \in \mathcal{N}_b} \bar{\lambda}_{nk} \mathbf{q}_{nk}^T & \sum_{n \in \mathcal{N}_a} \sum_{k \in \mathcal{N}_b} \bar{\lambda}_{nk} h_{nk} & \sum_{n \in \mathcal{N}_a} \sum_{k \in \mathcal{N}_b} \bar{\lambda}_{nk} + \Xi_B \end{bmatrix} \quad (81)$$

$$\mathbf{J}_{\mathbf{e}}^{\text{Array-B}} = \begin{bmatrix} N_a \sum_{k \in \mathcal{N}_b} \bar{\lambda}_{nk} \mathbf{J}_r(\bar{\phi}_k) + \Xi_{\mathbf{p}} & \mathbf{0} & N_a \sum_{k \in \mathcal{N}_b} \bar{\lambda}_k \bar{\mathbf{q}}_k \\ \mathbf{0}^T & \sum_{n \in \mathcal{N}_a} \sum_{k \in \mathcal{N}_b} \bar{\lambda}_k \bar{h}_{nk}^2 + \Xi_{\varphi} & 0 \\ N_a \sum_{k \in \mathcal{N}_b} \bar{\lambda}_k \bar{\mathbf{q}}_k^T & 0 & N_a \sum_{k \in \mathcal{N}_b} \bar{\lambda}_k + \Xi_{\mathbf{B}} \end{bmatrix} \quad (82)$$

ACKNOWLEDGMENTS

The authors would like to thank R. G. Gallager, A. Conti, H. Wymeersch, W. M. Gifford, and W. Suwansantisuk for their valuable suggestion and careful reading of the manuscript. We would also like to thank the anonymous reviewers for their constructive comments.

REFERENCES

- [1] A. Sayed, A. Tarighat, and N. Khajehnouri, "Network-based wireless location: challenges faced in developing techniques for accurate wireless location information," *IEEE Signal Process. Mag.*, vol. 22, no. 4, pp. 24–40, 2005.
- [2] K. Pahlavan, X. Li, and J. P. Makela, "Indoor geolocation science and technology," *IEEE Commun. Mag.*, vol. 40, no. 2, pp. 112–118, Feb. 2002.
- [3] J. J. Caffery and G. L. Stuber, "Overview of radiolocation in CDMA cellular systems," *IEEE Commun. Mag.*, vol. 36, no. 4, pp. 38–45, Apr. 1998.
- [4] N. Patwari, J. N. Ash, S. Kyperountas, A. O. Hero, III, R. L. Moses, and N. S. Correal, "Locating the nodes: cooperative localization in wireless sensor networks," *IEEE Signal Process. Mag.*, vol. 22, no. 4, pp. 54–69, Jul. 2005.
- [5] C.-Y. Chong and S. P. Kumar, "Sensor networks: evolution, opportunities, and challenges," *Proc. IEEE*, vol. 91, no. 8, pp. 1247–1256, Aug. 2003.
- [6] J. J. Spilker, Jr., "GPS signal structure and performance characteristics," *Journal of the Institute of Navigation*, vol. 25, no. 2, pp. 121–146, Summer 1978.
- [7] L. Kaplan, "Global node selection for localization in a distributed sensor network," *IEEE Transactions on Aerospace and Electronic Systems*, vol. 42, no. 1, pp. 113–135, 2006.
- [8] D. B. Jourdan, D. Dardari, and M. Z. Win, "Position error bound for UWB localization in dense cluttered environments," *IEEE Trans. Aerosp. Electron. Syst.*, vol. 44, no. 2, pp. 613–628, Apr. 2008.
- [9] S. Gezici, Z. Tian, G. B. Giannakis, H. Kobayashi, A. F. Molisch, H. V. Poor, and Z. Sahinoglu, "Localization via ultra-wideband radios: a look at positioning aspects for future sensor networks," *IEEE Signal Process. Mag.*, vol. 22, pp. 70–84, Jul. 2005.
- [10] C. Falsi, D. Dardari, L. Mucchi, and M. Z. Win, "Time of arrival estimation for UWB localizers in realistic environments," *EURASIP J. Appl. Signal Process.*, vol. 2006, pp. Article ID 32082, 1–13, 2006, special issue on *Wireless Location Technologies and Applications*.
- [11] Y. Shen and M. Z. Win, "Localization accuracy using wideband antenna arrays," *IEEE Trans. Commun.*, vol. 58, no. 1, pp. 270–280, Jan. 2010.
- [12] A. F. Molisch, "Ultra-wide-band propagation channels," *Proc. IEEE*, vol. 97, no. 2, pp. 353–371, Feb. 2009.
- [13] M. Z. Win and R. A. Scholtz, "Impulse radio: How it works," *IEEE Commun. Lett.*, vol. 2, no. 2, pp. 36–38, Feb. 1998.
- [14] —, "Characterization of ultra-wide bandwidth wireless indoor communications channel: A communication theoretic view," *IEEE J. Sel. Areas Commun.*, vol. 20, no. 9, pp. 1613–1627, Dec. 2002.
- [15] M. Z. Win, "A unified spectral analysis of generalized time-hopping spread-spectrum signals in the presence of timing jitter," *IEEE J. Sel. Areas Commun.*, vol. 20, no. 9, pp. 1664–1676, Dec. 2002.
- [16] Z. N. Low, J. H. Cheong, C. L. Law, W. T. Ng, and Y. J. Lee, "Pulse detection algorithm for line-of-sight (LOS) UWB ranging applications," *IEEE Antennas Wireless Propag. Lett.*, vol. 4, pp. 63–67, 2005.
- [17] Z. Zhang, C. L. Law, and Y. L. Guan, "BA-POC-Based ranging method with multipath mitigation," *IEEE Antennas Wireless Propag. Lett.*, vol. 4, pp. 492–495, 2005.
- [18] D. Dardari, C.-C. Chong, and M. Z. Win, "Threshold-based time-of-arrival estimators in UWB dense multipath channels," *IEEE Trans. Commun.*, vol. 56, no. 8, pp. 1366–1378, Aug. 2008.
- [19] D. Dardari, A. Conti, U. J. Ferner, A. Giorgetti, and M. Z. Win, "Ranging with ultrawide bandwidth signals in multipath environments," *Proc. IEEE*, vol. 97, no. 2, pp. 404–426, Feb. 2009, special issue on *Ultra-Wide Bandwidth (UWB) Technology & Emerging Applications*.
- [20] J.-Y. Lee and R. A. Scholtz, "Ranging in a dense multipath environment using an UWB radio link," *IEEE J. Sel. Areas Commun.*, vol. 20, no. 9, pp. 1677–1683, Dec. 2002.
- [21] A. F. Molisch, "Ultrawideband propagation channels-theory, measurements, and modeling," *IEEE Trans. Veh. Technol.*, vol. 54, no. 5, pp. 1528–1545, Sep. 2005.
- [22] M. Z. Win, G. Chrisikos, and N. R. Sollenberger, "Performance of Rake reception in dense multipath channels: Implications of spreading bandwidth and selection diversity order," *IEEE J. Sel. Areas Commun.*, vol. 18, no. 8, pp. 1516–1525, Aug. 2000.
- [23] L. Yang and G. B. Giannakis, "Ultra-wideband communications: an idea whose time has come," *IEEE Signal Process. Mag.*, vol. 21, no. 6, pp. 26–54, Nov. 2004.
- [24] T. Q. S. Quek and M. Z. Win, "Analysis of UWB transmitted-reference communication systems in dense multipath channels," *IEEE J. Sel. Areas Commun.*, vol. 23, no. 9, pp. 1863–1874, Sep. 2005.
- [25] W. Suwansantisuk, M. Z. Win, and L. A. Shepp, "On the performance of wide-bandwidth signal acquisition in dense multipath channels," *IEEE Trans. Veh. Technol.*, vol. 54, no. 5, pp. 1584–1594, Sep. 2005, special section on *Ultra-Wideband Wireless Communications—A New Horizon*.
- [26] A. F. Molisch, D. Cassioli, C.-C. Chong, S. Emami, A. Fort, B. Kannan, J. Karedal, J. Kunisch, H. Schantz, K. Siwiak, and M. Z. Win, "A comprehensive standardized model for ultrawideband propagation channels," *IEEE Trans. Antennas Propag.*, vol. 54, no. 11, pp. 3151–3166, Nov. 2006, special issue on *Wireless Communications*.
- [27] L. Mailaender, "On the geolocation bounds for round-trip time-of-arrival and all non-line-of-sight channels," *EURASIP Journal on Advances in Signal Processing*, vol. 2008, p. 10, 2008.
- [28] Y. Qi and H. Kobayashi, "Cramér-Rao lower bound for geolocation in non-line-of-sight environment," in *Proc. IEEE Int. Conf. Acoustics, Speech, and Signal Processing*, Orlando, FL, May 2002, pp. 2473–2476.
- [29] Y. Qi, H. Suda, and H. Kobayashi, "On time-of-arrival positioning in a multipath environment," in *Proc. IEEE Semiannual Veh. Technol. Conf.*, Los Angeles, CA, Sep. 2004, pp. 3540–3544.
- [30] Y. Qi, H. Kobayashi, and H. Suda, "Analysis of wireless geolocation in a non-line-of-sight environment," *IEEE Trans. Wireless Commun.*, vol. 5, no. 3, pp. 672–681, 2006.
- [31] J. Caffery, Ed., *Wireless Location in CDMA Cellular Radio Systems*. Boston, MA: Kluwer, 2000.
- [32] T. Rappaport, J. Reed, and B. Woerner, "Position location using wireless communications on highways of the future," *IEEE Commun. Mag.*, vol. 34, no. 10, pp. 33–41, 1996.
- [33] D. Niculescu and B. Nath, "Ad hoc positioning system (APS) using AOA," *Proc. IEEE Conf. on Computer Commun.*, vol. 3, pp. 1734–1743, Mar./Apr. 2003.
- [34] N. Patwari and A. O. Hero, III, "Using proximity and quantized RSS for sensor localization in wireless networks," *IEEE/ACM 2nd Workshop on Wireless Sensor Nets. & Applications*, pp. 20–29, 2003.
- [35] T. Pavani, G. Costa, M. Mazzotti, A. Conti, and D. Dardari, "Experimental results on indoor localization techniques through wireless sensors network," in *Proc. IEEE Semiannual Veh. Technol. Conf.*, vol. 2, May 2006, pp. 663–667.
- [36] A. F. Molisch, *Wireless Communications*, 1st ed. Piscataway, New Jersey, 08855-1331: IEEE Press, J. Wiley and Sons, 2005.
- [37] B. Van Veen and K. Buckley, "Beamforming: a versatile approach to spatial filtering," *IEEE Signal Process. Mag.*, vol. 5, no. 2, pp. 4–24, 1988.
- [38] H. Krim and M. Viberg, "Two decades of array signal processing research: the parametric approach," *IEEE Signal Process. Mag.*, vol. 13, no. 4, pp. 67–94, 1996.
- [39] R. Engelbrecht, "Passive source localization from spatially correlated angle-of-arrival data," *IEEE Trans. Signal Process.*, vol. 31, no. 4, pp. 842–846, 1983.

- [40] C.-C. Chong, C.-M. Tan, D. I. Laurenson, S. McLaughlin, M. A. Beach, and A. R. Nix, "A new statistical wideband spatio-temporal channel model for 5-GHz band WLAN systems," *IEEE J. Sel. Areas Commun.*, vol. 21, no. 2, pp. 139–150, Feb. 2003.
- [41] P. Deng and P. Fan, "An AOA assisted TOA positioning system," in *Proc. of Int. Conf. on Commun. Technol.*, vol. 2, Beijing, China, 2000, pp. 1501–1504.
- [42] L. Cong and W. Zhuang, "Hybrid TDOA/AOA mobile user location for wideband CDMA cellular systems," *IEEE Trans. Wireless Commun.*, vol. 1, no. 3, pp. 439–447, 2002.
- [43] C. Chang and A. Sahai, "Estimation bounds for localization," in *Proc. IEEE Conf. on Sensor and Ad Hoc Commun. and Networks*, S. Clara, CA, USA, Oct. 2004, pp. 415–424.
- [44] M. Hamilton and P. Schultheiss, "Passive ranging in multipath dominant environments. i. known multipath parameters," *IEEE Trans. Signal Process.*, vol. 40, no. 1, pp. 1–12, 1992.
- [45] J. Lee and S. Yoo, "Large error performance of UWB ranging," in *Proc. IEEE Int. Conf. on Ultra-Wideband (ICUWB)*, Zurich, Switzerland, 2005, pp. 308–313.
- [46] Y. Shen and M. Z. Win, "Fundamental limits of wideband localization accuracy via Fisher information," in *Proc. IEEE Wireless Commun. and Networking Conf.*, Kowloon, Hong Kong, Mar. 2007, pp. 3046–3051.
- [47] —, "Effect of path-overlap on localization accuracy in dense multipath environments," in *Proc. IEEE Int. Conf. on Commun.*, Beijing, China, May 2008, pp. 4197–4202.
- [48] M. Silventoinen and T. Rantalainen, "Mobile station emergency locating in GSM," in *Proc. of IEEE Int. Conf. on Personal Wireless Commun.*, New Delhi, 1996, pp. 232–238.
- [49] J. Caffery and G. Stuber, "Radio location in urban CDMA microcells," in *Proc. IEEE Int. Symp. on Personal, Indoor and Mobile Radio Commun.*, vol. 2, Toronto, Ont., 1995, pp. 858–862.
- [50] H. L. Van Trees, *Detection, Estimation and Modulation Theory*. New York, NY: Wiley, 1968, vol. 1.
- [51] H. V. Poor, *An Introduction to Signal Detection and Estimation*, 2nd ed. New York: Springer-Verlag, 1994.
- [52] M. Spirito, "On the accuracy of cellular mobile station location estimation," *IEEE Trans. Veh. Technol.*, vol. 50, no. 3, pp. 674–685, 2001.
- [53] M. Gavish and E. Fogel, "Effect of bias on bearing-only target location," *IEEE Trans. Aerosp. Electron. Syst.*, vol. 26, no. 1, pp. 22–26, Jan. 1990.
- [54] H. Koorapaty, H. Grubeck, and M. Cedervall, "Effect of biased measurement errors on accuracy of position location methods," in *Proc. IEEE Global Telecomm. Conf.*, vol. 3, Sydney, NSW, 1998, pp. 1497–1502.
- [55] M. Wylie and J. Holtzman, "The non-line of sight problem in mobile location estimation," in *Universal Personal Communications, 1996. Record., 1996 5th IEEE International Conference on*, vol. 2, Cambridge, MA, 1996, pp. 827–831.
- [56] S.-S. Woo, H.-R. You, and J.-S. Koh, "The NLOS mitigation technique for position location using IS-95CDMA networks," in *Proc. IEEE Semiannual Veh. Technol. Conf.*, vol. 6, Boston, MA, 2000, pp. 2556–2560.
- [57] S. Al-Jazzar, J. Caffery, J., and H.-R. You, "A scattering model based approach to NLOS mitigation in TOA location systems," in *Proc. IEEE Semiannual Veh. Technol. Conf.*, vol. 2, 2002, pp. 861–865.
- [58] P.-C. Chen, "A non-line-of-sight error mitigation algorithm in location estimation," in *Proc. IEEE Wireless Commun. and Networking Conf.*, vol. 1, Sep. 1999, pp. 316–320.
- [59] L. Xiong, "A selective model to suppress NLOS signals in angle-of-arrival (AOA) location estimation," in *Proc. 9th IEEE Int. Symp. on Personal, Indoor and Mobile Radio Communications*, vol. 1, Boston, MA, 1998, pp. 461–465.
- [60] H. Wang, L. Yip, K. Yao, and D. Estrin, "Lower bounds of localization uncertainty in sensor networks," in *Proc. IEEE Int. Conf. Acoustics, Speech, and Signal Processing*, Montreal, QC, May 2004, pp. 917–920.
- [61] M. Wax and A. Leshem, "Joint estimation of time delays and directions of arrival of multiple reflections of a known signal," *IEEE Trans. Signal Process.*, vol. 45, no. 10, pp. 2477–2484, Oct. 1997.
- [62] C. Botteron, A. Host-Madsen, and M. Fattouche, "Cramer-Rao bounds for the estimation of multipath parameters and mobiles' positions in asynchronous DS-SS systems," *IEEE Trans. Signal Process.*, vol. 52, no. 4, pp. 862–875, 2004.
- [63] Y. Shen, H. Wymeersch, and M. Z. Win, "Fundamental limits of wideband localization – Part II: Cooperative networks," *IEEE Trans. Inf. Theory*, vol. 56, 2010, to appear.
- [64] A. A. Saleh and R. A. Valenzuela, "A statistical model for indoor multipath propagation," *IEEE J. Sel. Areas Commun.*, vol. 5, no. 2, pp. 128–137, Feb. 1987.
- [65] I. Reuven and H. Messer, "A Barankin-type lower bound on the estimation error of a hybrid parameter vector," *IEEE Trans. Inf. Theory*, vol. 43, no. 3, pp. 1084–1093, May 1997.
- [66] R. A. Horn and C. R. Johnson, *Matrix Analysis*, 1st ed. Cambridge, NY: Cambridge University Press, 1985.
- [67] R. A. Scholtz, "How do you define bandwidth?" in *Proc. International Telemetry Conference*, Oct. 1972, pp. 281–288, Los Angeles, California, Invited Paper.
- [68] W. M. Lovelace and J. K. Townsend, "The effects of timing jitter and tracking on the performance of impulse radio," *IEEE J. Sel. Areas Commun.*, vol. 20, no. 9, pp. 1646–1651, Dec 2002.
- [69] S. W. Golomb and R. A. Scholtz, "Generalized Barker sequences," *IEEE Trans. Inf. Theory*, vol. IT-11, no. 4, pp. 533–537, Oct. 1965.
- [70] S. W. Golomb and M. Z. Win, "Recent results on polyphase sequences," *IEEE Trans. Inf. Theory*, vol. 44, no. 2, pp. 817–824, Mar. 1998.
- [71] S. W. Golomb and G. Gong, *Signal Design for Good Correlation: For Wireless Communication, Cryptography, and Radar*. Cambridge University Press, 2005.
- [72] D. Cassioli, M. Z. Win, and A. F. Molisch, "The ultra-wide bandwidth indoor channel: from statistical model to simulations," *IEEE J. Sel. Areas Commun.*, vol. 20, no. 6, pp. 1247–1257, Aug. 2002.

Yuan Shen (S'05) received his B.S. degree (with highest honor) from Tsinghua University, China, in 2005, and S.M. degree from the Massachusetts Institute of Technology (MIT) in 2008, both in electrical engineering.

Since 2005, he has been with Wireless Communications and Network Science Laboratory at MIT, where he is now a Ph.D. candidate. He was with the Hewlett-Packard Labs, CA, in winter 2009, the Corporate R&D of Qualcomm Inc., CA, in summer 2008, and the Intelligent Transportation Information System Laboratory, Tsinghua University, China, from 2003 to 2005. His research interests include communication theory, information theory, and statistical signal processing. His current research focuses on wideband localization, cooperative networks, and ultra-wide bandwidth communications.

Mr. Shen served as a member of the Technical Program Committee (TPC) for the IEEE Global Communications Conference (GLOBECOM) in 2010, the IEEE International Conference on Communications (ICC) in 2010, and the IEEE Wireless Communications & Networking Conference (WCNC) in 2009 and 2010. He received the Ernst A. Guillemin Thesis Award (first place) for the best S.M. thesis from the Department of Electrical Engineering and Computer Science at MIT in 2008, the Roberto Padovani Scholarship from Qualcomm Inc. in 2008, the Best Paper Award from the IEEE WCNC in 2007, and the Walter A. Rosenblith Presidential Fellowship from MIT in 2005.

Moe Z. Win (S'85-M'87-SM'97-F'04) received both the Ph.D. in Electrical Engineering and M.S. in Applied Mathematics as a Presidential Fellow at the University of Southern California (USC) in 1998. He received an M.S. in Electrical Engineering from USC in 1989, and a B.S. (*magna cum laude*) in Electrical Engineering from Texas A&M University in 1987.

Dr. Win is an Associate Professor at the Massachusetts Institute of Technology (MIT). Prior to joining MIT, he was at AT&T Research Laboratories for five years and at the Jet Propulsion Laboratory for seven years. His research encompasses developing fundamental theories, designing algorithms, and conducting experimentation for a broad range of real-world problems. His current research topics include location-aware networks, time-varying channels, multiple antenna systems, ultra-wide bandwidth systems, optical transmission systems, and space communications systems.

Professor Win is an IEEE Distinguished Lecturer and elected Fellow of the IEEE, cited for “contributions to wideband wireless transmission.” He was honored with the IEEE Eric E. Sumner Award (2006), an IEEE Technical Field Award for “pioneering contributions to ultra-wide band communications science and technology.” Together with students and colleagues, his papers have received several awards including the IEEE Communications Society’s Guglielmo Marconi Best Paper Award (2008) and the IEEE Antennas and Propagation Society’s Sergei A. Schelkunoff Transactions Prize Paper Award (2003). His other recognitions include the Laurea Honoris Causa from the University of Ferrara, Italy (2008), the Technical Recognition Award of the IEEE ComSoc Radio Communications Committee (2008), Wireless Educator of the Year Award (2007), the Fulbright Foundation Senior Scholar Lecturing and Research Fellowship (2004), the U.S. Presidential Early Career Award for Scientists and Engineers (2004), the AIAA Young Aerospace Engineer of the Year (2004), and the Office of Naval Research Young Investigator Award (2003).

Professor Win has been actively involved in organizing and chairing a number of international conferences. He served as the Technical Program Chair for the IEEE Wireless Communications and Networking Conference in 2009, the IEEE Conference on Ultra Wideband in 2006, the IEEE Communication Theory Symposia of ICC-2004 and Globecom-2000, and the IEEE Conference on Ultra Wideband Systems and Technologies in 2002; Technical Program Vice-Chair for the IEEE International Conference on Communications in 2002; and the Tutorial Chair for ICC-2009 and the IEEE Semiannual International Vehicular Technology Conference in Fall 2001. He was the chair (2004-2006) and secretary (2002-2004) for the Radio Communications Committee of the IEEE Communications Society. Dr. Win is currently an Editor for IEEE TRANSACTIONS ON WIRELESS COMMUNICATIONS. He served as Area Editor for *Modulation and Signal Design* (2003-2006), Editor for *Wideband Wireless and Diversity* (2003-2006), and Editor for *Equalization and Diversity* (1998-2003), all for the IEEE TRANSACTIONS ON COMMUNICATIONS. He was Guest-Editor for the PROCEEDINGS OF THE IEEE (Special Issue on UWB Technology & Emerging Applications) in 2009 and IEEE JOURNAL ON SELECTED AREAS IN COMMUNICATIONS (Special Issue on Ultra-Wideband Radio in Multiaccess Wireless Communications) in 2002.